
Learning 3D Anisotropic Noise Distributions Improves Molecular Force Field Modeling

Xixian Liu^{1*}, Rui Jiao^{2*}, Zhiyuan Liu^{3†}, Yurou Liu⁴, Yang Liu²,
 Ziheng Lu⁵, Wenbing Huang^{4†}, Yang Zhang³, Yixin Cao⁶

¹Fudan University, ²Tsinghua University, ³National University of Singapore

⁴Renmin University of China, ⁵Microsoft Research

⁶Institute of Trustworthy Embodied AI, Fudan University

xixian.liu@mila.quebec, jiaor21@mails.tsinghua.edu.cn

zhiyuan@nus.edu.sg, hwenbing@ruc.edu.cn

Abstract

Coordinate denoising has emerged as a promising method for 3D molecular pre-training due to its theoretical connection to learning a molecular force field. However, existing denoising methods rely on oversimplified molecular dynamics that assume atomic motions to be isotropic and homoscedastic. To address these limitations, we propose a novel denoising framework **AniDS**: Anisotropic Variational Autoencoder for 3D Molecular Denoising. AniDS introduces a structure-aware anisotropic noise generator that can produce atom-specific, full covariance matrices for Gaussian noise distributions to better reflect directional and structural variability in molecular systems. These covariances are derived from pairwise atomic interactions as anisotropic corrections to an isotropic base. Our design ensures that the resulting covariance matrices are symmetric, positive semi-definite, and $SO(3)$ -equivariant, while providing greater capacity to model complex molecular dynamics. Extensive experiments show that AniDS outperforms prior isotropic and homoscedastic denoising models and other leading methods on the MD17 and OC22 benchmarks, achieving average relative improvements of **8.9%** and **6.2%** in force prediction accuracy. Our case study on a crystal and molecule structure shows that AniDS adaptively suppresses noise along the bonding direction, consistent with physicochemical principles. Our code is available at <https://github.com/ZeroKnighting/AniDS>.

1 Introduction

Accurately and efficiently predicting atomic properties of molecules and materials is fundamental to a wide range of downstream applications, including drug discovery [1, 2], material design [3], catalyst design [4, 5], and molecular dynamics simulations [6, 7]. *Ab initio* methods such as Density Functional Theory (DFT) [8] are widely regarded as the standard for atomic property prediction, but their high computational cost significantly limits scalability to large systems or datasets. To overcome this challenge, machine learning potentials [9] have been developed to accelerate atomic simulations by orders of magnitude, with recent advances of graph neural networks (GNNs) [10, 11] further improving prediction accuracy. Among these methods, coordinate denoising [12, 13] has emerged as a promising training objective, due to its theoretical grounding in learning molecular force fields.

Classical coordinate denoising [12] involves recovering the original atomic coordinates \mathbf{X} from the perturbed version $\mathbf{X} + \epsilon$, where the noise $\epsilon \sim \mathcal{N}(\mathbf{0}, \sigma^2 \mathbf{I})$ is drawn from an isotropic Gaussian. This objective corresponds to learning the molecular force fields when the data distribution $p(\tilde{\mathbf{X}})$

*Equal contribution. † Correspondence.

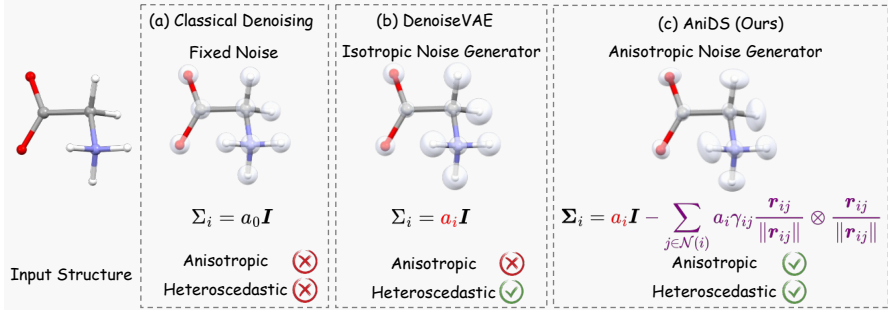


Figure 1: Comparison between different denoising approaches. The opaque spheres represent noise distributions. Our approach captures noise distribution that is both anisotropic and heteroscedastic.

is approximated as a mixture of isotropic Gaussians centered at each data point [13], *i.e.*, $p(\tilde{\mathbf{X}}) \approx \frac{1}{n} \sum_{i=1}^n \mathcal{N}(\tilde{\mathbf{X}}|\mathbf{X}_i, \sigma^2 \mathbf{I})$. A closer examination of this formulation reveals two implicit assumptions: (1) atomic motions are assumed to be **isotropic**, with identical variance along all axes ($\sigma_x^2 = \sigma_y^2 = \sigma_z^2$), ignoring direction-dependent stiffness such as bond stretching [14]; and (2) atomic motions are assumed to be **homoscedastic** [15], with all atoms sharing the same noise scale σ^2 , ignoring variability in energy potentials across distinct structures. While these assumptions make the implementation easier, they oversimplify the molecular dynamics, potentially leading to inaccurate force field learning.

Relaxing these assumptions demands a new noise distribution that is theoretically consistent with the assumed atomic motion. DenoiseVAE [16] learns adaptive noise scale σ^2 for different atoms, lifting the assumption of homoscedasticity, although the isotropic assumption remains less explored. On the other hand, earlier works [17, 18] move beyond isotropic Gaussian noises by introducing handcrafted noises, *e.g.*, perturbing bonds and dihedrals. However, these noises are applied independently at fixed scales, thus failing to address the assumption of homoscedasticity.

In this work, we propose a novel denoising framework: **Anisotropic Variational Autoencoder for 3D Molecular Denoising (AniDS)**, aiming to improve molecular force field learning by adaptively generating anisotropic Gaussian noises for coordinate denoising, thereby lifting all three assumptions discussed above. AniDS achieves this by adaptively generating a “full covariance matrix” (*i.e.*, without the diagonal constraint) for each atom’s Gaussian noise distribution, enabling it to capture directional variability and different molecular structures. However, generating such full covariance matrix introduces two major challenges that have hindered prior efforts: (1) Ensuring the covariance matrices are symmetric, positive semi-definite, and equivariant, which are fundamental properties of covariance matrices and molecules. While these properties are trivially satisfied in isotropic settings, they require explicit modeling and constraint in the anisotropic case. (2) Guiding the covariance learning process with proper physicochemical priors. The space of full covariance matrices is high-dimensional and susceptible to trivial or degenerated solutions if not properly regularized, which often leads to unstable or failed pretraining.

To address these challenges, AniDS introduces a **structure-aware anisotropic noise generator** that leverages 3D molecular structures to produce atom-specific full covariance matrices for anisotropic noise distributions. Specifically, the generator first constructs an isotropic base term and then applies anisotropic corrections derived from the learned pairwise atomic interactions. These anisotropic corrections enable the model to capture local rigidity and directional variability across different molecular structures, acting as a physicochemical prior. Additionally, our design ensures the covariance matrices are symmetric, positive semi-definite, and $\text{SO}(3)$ -equivariant. Equipped with this expressive noise generator, AniDS supervises a molecular denoising autoencoder using our theoretically grounded denoising loss that approximates learning the molecular force field.

AniDS achieves an average relative improvement of **8.9%** on MD17 and **6.2%** on OC22 in force prediction. Ablation studies confirm the effectiveness of each component. Our case study further shows that AniDS adaptively adjusts the direction and scale of the noise according to the atomic interactions’ strength in $\text{H}_3\text{In}_{12}\text{O}_{48}\text{Pd}_{12}$ and SNPH_4 structures, aligning with physicochemical principles.

2 Preliminary: Coordinate Denoising and DenoiseVAE

We begin by introducing the coordinate denoising [13] objective and the subsequent study DenoiseVAE [16] that addresses the homoscedastic assumption.

Notation of Molecules. In this work, we develop a framework to learn force fields for both small molecules and crystal materials. For clarity, we present the methodology using the notation of small molecules; the extension to crystals is straightforward and involves revising the denoising autoencoder to reflect crystals’ periodicity. Details of this adaptation are provided in Appendix B.

A 3D molecule $\mathbf{M} = (\mathbf{Z}, \mathbf{X}, \mathbf{E})$ is represented by: (1) $\mathbf{Z} \in \mathbb{N}^N$, with $\mathbf{Z}_i \in \mathbb{N}$ denotes the atomic number of the i -th atom; (2) $\mathbf{X} \in \mathbb{R}^{N \times 3}$, where $\mathbf{X}_i \in \mathbb{R}^3$ specifies the 3D coordinates of the i -th atom; and (3) $\mathbf{E} \in \mathbb{R}^{N \times N \times d}$, where $\mathbf{E}_{ij} \in \mathbb{R}^d$ denotes the bond existence and bond type between atoms i and j . Here, N denotes the number of atoms in the molecule.

Coordinate Denoising. Given a molecule \mathbf{M} in equilibrium, in which the atom-wise forces are near zero, a corrupted version is generated as $\tilde{\mathbf{M}} = (\mathbf{Z}, \tilde{\mathbf{X}}, \mathbf{O})$, where the atomic coordinates are perturbed by Gaussian noise: $\tilde{\mathbf{X}} = \mathbf{X} + \sigma \epsilon$ with $\epsilon \sim \mathcal{N}(\mathbf{0}, \mathbf{I})$. Here σ is a hyperparameter controlling the added noise scale, which is usually around 0.1 to generate a small perturbation. Then, a denoising autoencoder [19–21] $\phi(\cdot)$ is trained to predict the added noise by minimizing the following loss: $\mathbb{E}_{p(\tilde{\mathbf{M}}, \mathbf{M})} \|\phi(\tilde{\mathbf{M}}) - (\tilde{\mathbf{X}} - \mathbf{X})/\sigma^2\|^2$. Theoretically, this denoising objective is shown to approximate learning a molecular force field [13], therefore improving its performance.

DenoiseVAE [16]. The standard coordinate denoising operates under the homoscedasticity assumption, treating all atoms equally. Specifically, a fixed noise scale σ is used to simulate minor thermal fluctuations for all atoms, but fails to capture the energy variations across different molecular structures. For example, in a rigid structure like a benzene ring, a minor coordinate perturbation can lead to a disproportionately large energy change, whereas similar perturbations in more flexible regions may have negligible energetic impact. Resolving this issue, DenoiseVAE trains a noise generator $\psi(\cdot)$ to adaptively assign a distinct noise scale σ_i to each atom based on the molecular structure:

$$\{\sigma_i \in \mathbb{R}^+ \mid i \in \mathbf{M}\} = \psi(\mathbf{M}), \quad (1) \quad \tilde{\mathbf{X}}_i = \mathbf{X}_i + \sigma_i \epsilon_i, \quad \epsilon_i \sim \mathcal{N}(\mathbf{0}, \mathbf{I}). \quad (2)$$

We then obtain the perturbed molecule $\tilde{\mathbf{M}} = (\mathbf{Z}, \tilde{\mathbf{X}}, \mathbf{L})$, and perform denoise training as follows:

$$\mathcal{L}_{\text{Denoise}} = \frac{1}{|\mathbf{M}|} \mathbb{E}_{p(\tilde{\mathbf{X}}, \mathbf{X})} \sum_{i \in \mathbf{M}} \sigma_i^2 \|\phi(\tilde{\mathbf{M}}) - \frac{(\tilde{\mathbf{X}} - \mathbf{X})}{\sigma_i^2}\|^2, \quad (3)$$

$$\mathcal{L}_{\text{KL}} = \frac{1}{|\mathbf{M}|} \sum_{i \in \mathbf{M}} \mathbf{D}_{\text{KL}}(\mathcal{N}(\mathbf{0}, \sigma_i^2 \mathbf{I}) \parallel p_i), \quad (4)$$

where p_i is the prior distribution, set to $\mathcal{N}(\mathbf{0}, \sigma_p^2 \mathbf{I})$, and σ_p is a hyperparameter. The KL divergence term \mathcal{L}_{KL} acts as a regularizer to prevent the noise generator $\psi(\cdot)$ from collapsing to trivial solutions where $\sigma_i \rightarrow 0$. This ensures meaningful denoise training. The final training objective combines both losses $\mathcal{L}_{\text{DenoiseVAE}} = \lambda_{\text{Denoise}} \mathcal{L}_{\text{Denoise}} + \lambda_{\text{KL}} \mathcal{L}_{\text{KL}}$ with balancing coefficients λ_{Denoise} and λ_{KL} .

3 Methodology

In this section, we start by overviewing the AniDS framework. We then present the motivations and detailed formulations of its key components in Sections 3.2 and Section 3.3, respectively. Finally, we describe how AniDS can be adapted to different training schemes in Section 3.4.

3.1 Overview of the AniDS Framework

AniDS consists of three key components: (1) a structure-aware anisotropic noise generator $\psi(\cdot)$ that generates per-atom noise distribution conditioned on the molecule structure \mathbf{M} ; (2) a denoising autoencoder $\phi(\cdot)$ that is trained for coordinate denoising; and (3) a denoising objective $\mathcal{L}_{\text{AniDS}}$ that approximates learning molecular force field.

Structure-aware Anisotropic Noise Generator. Given a molecule \mathbf{M} , AniDS employs a noise generator $\psi(\cdot)$ to generate a full covariance matrix $\Sigma_i \in \mathbb{R}^{3 \times 3}$ for each atom $i \in \mathbf{M}$, defining an anisotropic Gaussian noise distribution $\mathcal{N}(\mathbf{0}, \Sigma_i)$. Unlike prior works that assume diagonal Σ_i for theoretical and computational convenience [22, 13], AniDS models Σ_i as a dense matrix to capture directional variability. To ensure that the generated noise reflects the underlying molecular structure, $\psi(\cdot)$ should be implemented with structure-aware molecular encoders [23, 24]. This enables the generated covariance matrices to reflect local and global molecular structural contexts. Given this generator $\psi(\cdot)$, the perturbed molecule $\tilde{\mathbf{M}}$ can be obtained as:

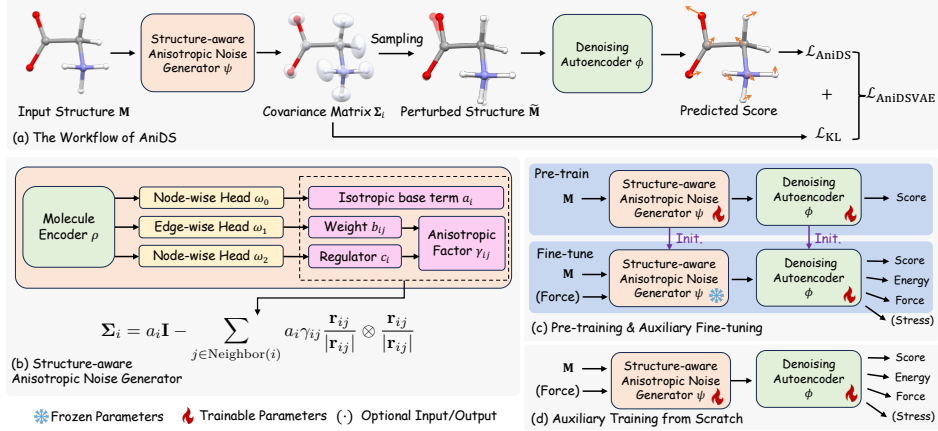


Figure 2: Overview of the AniDS framework.

$$\{\Sigma_i \in \mathbb{R}^{3 \times 3} | i \in \mathbf{M}\} = \psi(\mathbf{M}), \quad (5)$$

$$\tilde{\mathbf{X}}_i = \mathbf{X}_i + \mathbf{L}_i \epsilon_i, \epsilon_i \sim \mathcal{N}(\mathbf{0}, \mathbf{I}), \quad (7)$$

$$\mathbf{L}_i = \text{Cholesky}(\Sigma_i), \quad (6)$$

$$\tilde{\mathbf{M}} = (\mathbf{Z}, \tilde{\mathbf{X}}, \mathbf{E}), \quad (8)$$

where $\tilde{\mathbf{X}}_i$ is the perturbed coordinate of the i -th atom, sampled via Cholesky decomposition [25] of the learned covariance Σ_i . While the noise generator can be any neural network capable of producing symmetric, positive semi-definite, and 3D-equivariant covariance matrices, we introduce our implementation in Section 3.2.

Denoising Autoencoder. The denoising autoencoder ϕ takes the perturbed structure $\tilde{\mathbf{M}}$ as input and predicts atom-wise vectors intended to recover the original coordinates: $\phi(\tilde{\mathbf{M}}) \in \mathbb{R}^{N \times 3}$. AniDS is a model-agnostic framework that can be integrated into a wide range of molecular backbones. In this work, we implement ϕ with EquiformerV2 [24] and Geoformer [26], which have demonstrated strong performance on molecular benchmarks. To enable coordinate denoising on non-equilibrium structures, we follow [27] to include **force encoding** as the additional features for the corrupted atoms. Unlike equilibrium structures, which are uniquely defined by local energy minima, multiple non-equilibrium structures may share the same energy level, introducing ambiguity into the denoising targets. Including force information helps disambiguate these cases by anchoring the target to a specific molecular state. Our detailed implementations of the denoising autoencoders and the force encoding are introduced in Appendix B.1.

AniDS’s Denoising Objective. AniDS’s denoising loss jointly trains the noise generator and the denoising autoencoder to recover the noise vector scaled by the inverse covariance:

$$\mathcal{L}_{\text{AniDS}} = \frac{1}{|\mathbf{M}|} \mathbb{E}_{q_{\Sigma}(\tilde{\mathbf{X}}, \mathbf{X})} \sum_{i \in \mathbf{M}} \left\| \phi(\tilde{\mathbf{M}})_i - [\Sigma_i]^{-1} (\tilde{\mathbf{X}}_i - \mathbf{X}_i) \right\|^2. \quad (9)$$

We show in Section 3.3 that the objective above approximates learning the molecular force field. Additionally, we compute a KL divergence loss between the learned anisotropic noise distribution and an isotropic Gaussian prior $\mathcal{N}(0, \sigma_p^2 I)$:

$$\mathcal{L}_{\text{KL}} = \frac{1}{2|\mathbf{M}|} \sum_{i \in \mathbf{M}} \left(\text{tr}(\sigma_p^{-2} \Sigma_i) - d + \ln \frac{|\sigma_p^2 I|}{|\Sigma_i|} \right), \quad (10)$$

which prevents the learned covariance from collapsing into trivial solutions like zeros. Recall that the normalized anisotropic weights $\{\gamma_{ij}\}$ on Eq. 15 satisfy $\sum_j \gamma_{ij} < 1$ by construction. To avoid degenerate covariances that become overly isotropic in flexible regions, we regularize the total anisotropic mass $\Gamma_i := \sum_j \gamma_{ij}$ towards a target level $\kappa \in (0, 1)$ via a one-sided hinge-squared penalty:

$$\mathcal{L}_{\gamma} = \frac{1}{|\mathbf{M}|} \sum_{i \in \mathbf{M}} [\max(0, \kappa - \Gamma_i)]^2. \quad (11)$$

Intuitively, Eq. (11) discourages vanishing anisotropic corrections (i.e., Γ_i too small), while preserving the PSD guarantee $\Gamma_i < 1$ from 15. The final loss $\mathcal{L}_{\text{AniDSVAE}}$ is a weighted sum of the denoising and regularization terms:

$$\mathcal{L}_{\text{AniDS-VAE}} = \lambda_{\text{AniDS}} \mathcal{L}_{\text{AniDS}} + \lambda_{\text{KL}} \mathcal{L}_{\text{KL}} + \lambda_{\gamma} \mathcal{L}_{\gamma}. \quad (12)$$

3.2 Structure-Aware Anisotropic Noise Generation

The noise generator $\psi(\cdot)$ constructs symmetric, positive semi-definite, and $\text{SO}(3)$ -equivariant covariance matrices $\{\Sigma_i | i \in \mathbf{M}\}$. These matrices encode both isotropic and anisotropic uncertainty in atomic positions, reflecting each atom's structural context. The generation consists of two main steps:

Atom-wise Structural Representation. A molecular structure encoder $\rho(\cdot)$ is used to extract structural representations, to guide the covariance generation process. This work shares the architecture as the denoising autoencoder. Formally, we have:

$$\{\mathbf{h}_i \in \mathbb{R}^d | i \in \mathbf{M}\} = \rho(\mathbf{M}), \quad (13)$$

where \mathbf{h}_i encodes the structural and chemical contexts of atom i .

Covariance Matrix. Given the structural representation above, we parameterize the covariance matrix Σ_i for atom i as the sum of a isotropic base term and an anisotropic term, motivated by our physicochemical prior of pairwise atomic interactions:

$$\Sigma_i = \underbrace{a_i \mathbf{I}}_{\text{Isotropic Base}} - \underbrace{\sum_{j \in \text{Neighbor}(i)} a_i \gamma_{ij} \frac{\mathbf{r}_{ij}}{|\mathbf{r}_{ij}|} \otimes \frac{\mathbf{r}_{ij}}{|\mathbf{r}_{ij}|}}_{\text{Anisotropic Corrections}}, \quad (14)$$

$$\gamma_{ij} = \frac{\exp(b_{ij})}{\sum_{l \in \text{Neighbor}(i)} \exp(b_{il}) + c_i} \quad (\text{Normalized anisotropic weight}), \quad (15)$$

where $\mathbf{r}_{ij} = \mathbf{X}_i - \mathbf{X}_j \in \mathbb{R}^3$ is the relative position vector. The parameters a_i , b_{ij} , and c_i are adaptively derived from the atomic structural representations $\{\mathbf{h}_i | i \in \mathbf{M}\}$ using MLPs (*i.e.*, ω_0 , ω_1 , and ω_2) and a radial basis function [28] $\eta(\cdot)$, respectively:

- **Isotropic base term** $a_i = \exp(\omega_0(\mathbf{h}_i)) \in \mathbb{R}^+$. It controls the baseline noise level for atom i , reflecting its intrinsic flexibility. Larger a_i values indicate greater isotropic flexibility.
- **Anisotropic weight** $b_{ij} = \omega_1([\mathbf{h}_i; \mathbf{h}_j; \eta(|\mathbf{r}_{ij}|)]) \in \mathbb{R}$. It controls the weights of anisotropic corrections, which determines the directional stiffness between atoms i and j . For example, along covalent bonds, high b_{ij} produces high γ_{ij} that suppresses motion along \mathbf{r}_{ij} . Conversely, $b_{ij} \ll 0$ for distant atom pairs eliminates the corresponding directional influence of stiffness.
- **Anisotropic regulator** $c_i = \exp(\omega_2(\mathbf{h}_i)) \in \mathbb{R}^+$. It regulates the influence of anisotropic corrections. In symmetric or rigid environments, such as aromatic rings, larger c_i values suppress individual directional components, resulting in a more isotropic noise distribution. In contrast, smaller c_i allows stronger anisotropic corrections to reflect local uncertainty in flexible regions.

Our noise generator is designed to ensure three essential properties of the covariance matrix:

- **Symmetry:** $\Sigma_i = \Sigma_i^\top$ is satisfied due to the symmetry of the isotropic base and the outer product.
- **Positive Semi-Definiteness:** The covariance matrix is positive definite ($\Sigma_i \succ 0$) if $\sum_j \gamma_{ij} < 1$, enforced via the softmax in Equation (15). This condition guarantees the anisotropic correction term does not overpower the isotropic base $a_i \mathbf{I}$. A detailed proof is in Appendix B.
- **SO(3)-Equivariance and T(3)-Invariance:** Given $\text{SE}(3)$ transformation $g = (\mathbf{R}, \mathbf{t})$ of rotation $\mathbf{R} \in \text{SO}(3)$ and translation $\mathbf{t} \in \mathbb{R}^3$ applied on the molecule \mathbf{M} , the transformed covariance matrix satisfies $g \circ \Sigma_i = \mathbf{R} \Sigma_i \mathbf{R}^\top$: the covariance matrix is equivariant to the rotation but invariant to the translation. This is because the translation is canceled out when computing $\mathbf{r}_{ij} = \mathbf{X}_i - \mathbf{X}_j$.

3.3 AniDS Learns Molecular Force Fields

Here, we show that AniDS's denoising objective approximates learning molecular force field.

Step 1: Boltzmann Distribution and Gaussian Mixture Approximation. The distribution of molecular structures follows the Boltzmann distribution: $p_{\text{physical}}(\tilde{\mathbf{X}}) \propto \exp(-\frac{E(\tilde{\mathbf{X}})}{k_B T})$, where $E(\tilde{\mathbf{X}})$ is the potential energy. Following prior works [13, 29], we approximate p_{physical} as a mixture of Gaussians centered at the known structures, typically selected as the equilibrium conformations [13]. Subsequent study [17] demonstrates that learning this Gaussian mixture over non-equilibrium structures is theoretically equivalent to modeling a hybrid noise distribution over equilibrium ones (See

Proposition 3.4 in [17]). In their work, non-equilibrium structures are generated by applying small torsional perturbations to equilibrium conformations. Further studies show that intermediate states from molecular dynamics simulations can also serve as effective non-equilibrium samples for denoising [22, 27], which are also adopted in our work. Specifically, we have:

$$p_{\text{physical}}(\tilde{\mathbf{X}}) \approx q_{\Sigma}(\tilde{\mathbf{X}}) = \frac{1}{|\mathcal{D}|} \sum_{k=1}^{|\mathcal{D}|} q_{\Sigma}(\tilde{\mathbf{X}}|\mathbf{X}^{(k)}), \quad (16)$$

where $\mathbf{X}^{(k)}$ is the k -th structure in dataset \mathcal{D} . We define $q_{\Sigma}(\tilde{\mathbf{X}}|\mathbf{X}^{(k)}) = \prod_{i=1}^N \mathcal{N}(\tilde{\mathbf{X}}_i; \mathbf{X}_i^{(k)}, \Sigma_i^{(k)})$. Here $\mathbf{X}_i^{(k)} \in \mathbb{R}^3$ denotes the coordinate of the i -th atom in the k -th structure, and $\Sigma_i^{(k)} \in \mathbb{R}^{3 \times 3}$ is the covariance matrix of the i -th atom in the k -th structure.

Step 2: Score Function of the Gaussian Mixture. The score (gradient of the log-density) is:

$$\nabla_{\tilde{\mathbf{X}}} \log q_{\Sigma}(\tilde{\mathbf{X}}) = \frac{\sum_{k=1}^{|\mathcal{D}|} q_{\Sigma}(\tilde{\mathbf{X}}|\mathbf{X}^{(k)}) \nabla_{\tilde{\mathbf{X}}} \log q_{\Sigma}(\tilde{\mathbf{X}}|\mathbf{X}^{(k)})}{\sum_{k=1}^{|\mathcal{D}|} q_{\Sigma}(\tilde{\mathbf{X}}|\mathbf{X}^{(k)})} \quad (17)$$

Step 3: Link to Molecular Force Field. Under the Boltzmann distribution, the force field is proportional to the score:

$$\mathbf{F}(\tilde{\mathbf{X}}) = -\nabla_{\tilde{\mathbf{X}}} E(\tilde{\mathbf{X}}) = k_B T \cdot \nabla_{\tilde{\mathbf{X}}} \log p_{\text{physical}}(\tilde{\mathbf{X}}). \quad (18)$$

For small perturbation ($\tilde{\mathbf{X}} \approx \mathbf{X}^{(k)}$), the Gaussian mixture is dominated by the nearest structure $\mathbf{X}^{(k)}$, simplifying the score (cf. Equation (17)) to:

$$\nabla_{\tilde{\mathbf{X}}} \log q_{\Sigma}(\tilde{\mathbf{X}}) \approx \nabla_{\tilde{\mathbf{X}}} \log q_{\Sigma}(\tilde{\mathbf{X}}|\mathbf{X}^{(k)}) = -\sum_{j=1}^N [\Sigma_i^{(k)}]^{-1} (\tilde{\mathbf{X}}_i - \mathbf{X}_i^{(k)}). \quad (19)$$

Substituting this into the force field expression (cf. Equation (18)), we identify:

$$\mathbf{F}(\tilde{\mathbf{X}}) \propto \sum_{i=1}^N [\Sigma_i^{(k)}]^{-1} (\tilde{\mathbf{X}}_i - \mathbf{X}_i^{(k)}). \quad (20)$$

Step 4: Denoising as Learning Force Field. AniDS trains a denoise autoencoder $\phi(\tilde{\mathbf{M}})$ to predict the noise scaled by the inverse covariance (cf. Equation (9)). By Vincent’s theorem [30], this is equivalent to score matching:

$$\mathcal{L}_{\text{AniDS}} \propto \mathbb{E}_{q_{\Sigma}(\tilde{\mathbf{X}})} \|\phi(\tilde{\mathbf{M}}) - \nabla_{\tilde{\mathbf{X}}} \log q_{\Sigma}(\tilde{\mathbf{X}})\|^2 \quad (21)$$

At convergence, $\phi^*(\tilde{\mathbf{M}}) = \nabla_{\tilde{\mathbf{X}}} \log q_{\Sigma}(\tilde{\mathbf{X}}) \approx \nabla_{\tilde{\mathbf{X}}} \log p_{\text{physical}}(\tilde{\mathbf{X}})$, recovering the force field: $\phi^*(\tilde{\mathbf{M}}) \propto -\mathbf{F}(\tilde{\mathbf{X}})$. Prior works of Coordinate Denoising [27] and DenoiseVAE [16] can be seen as special cases of our approach, with detailed derivations provided in Appendix B.

3.4 Adapting AniDS to Different Training Schemes

Consistent with prior works, we adopt AniDS under two training schemes: (1) as a pretraining objective followed by task-specific fine-tuning [13, 31], and (2) as an auxiliary task jointly optimized with supervised force field learning when training from scratch [27, 12].

Pre-training and Fine-tuning. Following [12, 31], we can apply AniDS (cf. Equation (12)) to pretrain the denoising autoencoder ϕ and the structure-aware noise generator ψ altogether on a large pretraining dataset. The pretrained encoder ϕ is then fine-tuned on downstream datasets for supervised force field learning, with the AniDS objective retained as an auxiliary loss, as described in the following paragraph. During fine-tuning, the parameters of the noise generator ψ are kept frozen.

Supervised Learning with Partial Corruption and Auxiliary Denoising. We use AniDS as an auxiliary loss for supervised force field learning. Inspired by [27], we adopt a partially corrupted denoising strategy. Specifically, only a subset of a molecule’s atom coordinates is corrupted using the noise generator. The model is trained with the weighted sum of supervised force field loss on the uncorrupted atoms and AniDS loss (cf. Equation (12)) on the corrupted atoms. This design ensures that the model learns from clean ground truth coordinates for supervised force field learning, while still benefiting from denoising regularization. Compared to corrupting all the atoms, this method mitigates the mismatch between the the ground truth force field label and the perturbed structure. Implementation details are provided in Appendix B.3.

Table 1: MAE for force prediction on MD17’s test sets. Forces are reported in units of kcal/mol. Bold numbers indicate the best performance. **Green** denotes relative improvement to the baseline.

Model	Aspirin	Benzene	Ethanol	Malonaldehyde	Naphthalene	Salicylic Acid	Toluene	Uracil	Avg
SchNet [37]	1.35	0.31	0.39	0.66	0.58	0.85	0.57	0.56	0.66
DimeNet [38]	0.499	0.187	0.230	0.383	0.215	0.374	0.216	0.301	0.300
PaIINN [39]	0.338	-	0.224	0.319	0.077	0.195	0.094	0.139	-
TorchMD-NET [40]	0.253	0.196	0.109	0.169	0.061	0.129	0.067	0.095	0.135
NequIP (Lmax=3) [10]	0.184	-	0.071	0.129	0.039	0.090	0.046	0.076	-
SE(3)-DDM [41]	0.453	-	0.166	0.288	0.129	0.266	0.122	0.122	-
Coord [13]	0.211	0.169	0.096	0.139	0.053	0.109	0.058	0.074	0.114
Frad [17]	0.209	0.199	0.091	0.1415	0.053	0.108	0.054	0.076	0.116
Slide [18]	0.174	0.169	0.088	0.153	0.048	0.100	0.054	0.082	0.109
DeNS [27] (Lmax=2)	0.131	0.141	0.060	0.101	0.039	0.085	0.044	0.076	0.085
DeNS [27] (Lmax=3)	0.120	0.141	0.055	0.095	0.037	0.074	0.042	0.067	0.079
AniDS (Lmax=2)	0.102 <small>+15.0%</small>	0.139 <small>+1.4%</small>	0.050 <small>+9.1%</small>	0.084 <small>+11.6%</small>	0.036 <small>+2.7%</small>	0.064 <small>+13.5%</small>	0.038 <small>+9.5%</small>	0.062 <small>+7.5%</small>	0.072 <small>+8.9%</small>

Table 2: Performance comparison on OC22’s S2EF-Total validation set.

Model	Params	Energy E-MAE (meV)			Force F-MAE (meV/Å)		
		ID	OOD	Avg	ID	OOD	Avg
GemNet-OC [42]	39M	545	1011	778	30.0	40.0	35.0
GemNet-OC (OC20+OC22) [42]	39M	464	859	661.5	27.0	34.0	30.5
E2former [43]	67M	491	724	607.5	25.98	36.45	31.22
EquiformerV2 [24]	122M	433.0	629.0	531	22.88	30.70	26.79
EquiformerV2 + DeNS [27]	127M	391.6	533.0	462.3	20.66	27.11	23.89
EquiformerV2 + AniDS (ours)	129M	370.0 <small>+5.5%</small>	525.4 <small>+1.4%</small>	447.7 <small>+3.2%</small>	19.53 <small>+5.5%</small>	25.27 <small>+6.8%</small>	22.4 <small>+6.2%</small>

4 Experiments

Datasets. We briefly describe the datasets in our experiments, and leave additional setup details in Appendix C.2. Our experiments involve four datasets: (1) **PCQM4Mv2** [32] contains 3,746,619 molecules along with their Density Functional Theory (DFT) calculated 3D equilibrium structures. (2) **OC22** [33] is a large-scale dataset of DFT calculated structures designed to advance machine learning for oxide electrocatalysts. (3) **MD17** [34] provides molecular dynamics trajectories of small organic molecules, with both energy and force labels. (4) **MPtrj** [35] includes 1.58 million structures obtained from DFT relaxation trajectories of over 146,000 materials in the Materials Project [36].

4.1 Results of pre-training and Fine-tuning

Setup. We pre-train our model on PCQM4Mv2 and subsequently fine-tune it exclusively on MD17. We adopt the Equiformer-V2 backbone [24]. Note, we use only the 3D structures without the property values in PCQM4Mv2. During the fine-tuning, given that the pre-trained AniDS has already learned a decent distribution for adding noise, we freeze the noise generator and only train the denoising autoencoder, using AniDS as an auxiliary task along with supervised learning. Following [27], we use 950 molecules for training and 50 for testing. No noise is added during validation and testing.

MD17. Table 1 presents the results on MD17. Our method achieves the best across all evaluated tasks. Compared to the previous results, we observe an average improvement of approximately **8.9%** across the tasks. We attribute this significant improvement to our structure-aware noise generator, which produces anisotropic noise, enabling our model to learn the molecular potential energy surface more effectively. Furthermore, while DeNS ($L_{max} = 3$) enhances input features by increasing the degree of irreducible representations in EquiformerV2, AniDS ($L_{max} = 2$) outperforms it while using a lower dimensional irreducible representation. This demonstrates the efficacy of our adaptive structure-driven noise sampling strategy, suggesting that well-informed noise learning can lead to a more generalizable force field prediction.

4.2 Results of Supervised Learning with Partial Corruption and Auxiliary Denoising

Setup. Here AniDS is used as an auxiliary task when conducting supervised learning on OC22. Due to resource constraints, we adopt the pre-trained models from [27]. This pre-trained model utilizes the EquiformerV2 architecture, and its training process incorporated DeNS as an auxiliary task. Given its architectural similarity to the model used for MD17, we can easily extend its training by integrating our AniDS framework. Following [27], we conduct training on OC22’s S2EF-Total task, which contains 8.2 million structures. We further evaluate performance on the provided validation split [33]. Additionally, our results on MPTrj are provided in Appendix C.

Table 3: Ablation Studies on the Aspirin dataset of MD17. **(a)** Comparison of different denoising methods under the pre-train-fine-tune scheme. **(b)** Comparison of different denoising methods under the pre-train-fine-tune scheme. Standard supervised fine-tuning is used without AniDS as an auxiliary task. **(c)** Hyperparameter analysis under the pre-train and fine-tune scheme.

(a) Pre-train and Fine-tune		(b) w/o Auxiliary Fine-tuning		(c) Hyperparameters	
Model	F(MAE)	Model	F(MAE)	EqV2	F(MAE)
–	–	–	–	$\sigma_p = 0.5$	0.13018
EqV2-No pre-train	0.1929	EqV2-No pre-train	0.1929	$\sigma_p = 0.1$	0.11180
EqV2-DeNS	0.1178	EqV2-DeNS	0.1424	$\sigma_p = 0.05$	0.11594
EqV2-DenoiseVAE	0.1143	EqV2-DenoiseVAE	0.1400	$\lambda_{KL} = 1.5$	0.11714
EqV2-AniDS-add	0.1128	EqV2-AniDS-add	0.1389	$\lambda_{KL} = 1.0$	0.11180
EqV2-AniDS	0.1118	EqV2-AniDS	0.1369	$\lambda_{KL} = 0.5$	0.11461

OC22. Table 2 presents the results. Compared to baselines, AniDS achieves state-of-the-art performance across all tasks. This is because AniDS can more accurately generate noise that aligns with the atomic vibration modes, thereby better assisting the model to learn molecular force fields. Notably, our model demonstrates an improvement of $\sim 3.2\%$ in energy prediction for both the in-distribution (ID) and out-of-distribution (OOD) datasets, and an improvement of $\sim 6.2\%$ in force prediction for both ID and OOD datasets. These superior results underscore the effectiveness of our method.

4.3 Ablation Study and Hyperparameter Analysis

Impact of Different Denoising Methods. We evaluate various denoising strategies with the same Equiformer-v2 backbone [24], pre-trained on the PCQM4Mv2 dataset. The methods include: (1) no pre-training; (2) denoise training with fixed-scale isotropic Gaussian Noise (EqV2-DeNS [27]); (3) DenoiseVAE [16]; (4) AniDS with additive anisotropic correction instead of subtractive correction (*cf.* Equation 14; EqV2-AniDS-add); and (5) our method AniDS.

Table 3 compares two fine-tuning settings following denoising pre-training: (a) fine-tuning with denoising as an auxiliary task, and (b) fine-tuning without denoising. In both settings, our model consistently outperforms all baselines. All denoising-based pre-training methods substantially outperform the baseline without pre-training, supporting the benefit of learning molecular noise distributions. Notably, models using anisotropic noise (EqV2-AniDS and EqV2-AniDS-add) consistently outperform those using isotropic noise (EqV2-DeNS and EqV2-DenoiseVAE), confirming that isotropic assumptions oversimplify molecular dynamics. Moreover, the subtractive correction in EqV2-AniDS yields slightly better results than the additive correction in EqV2-AniDS-add, suggesting that incorporating directional stiffness from physicochemical priors improves the model’s structural understanding.

Impact of Different σ_p and λ_{KL} . The choice of prior distribution σ_p and the strength of the KL loss λ_{KL} both affect model performance. As shown in Table 3(c) (top), varying σ_p influences how effectively the model learns from the noise prior, with the best performance achieved at $\sigma = 0.1$. In addition, Table 3c (bottom) shows the effect of different λ_{KL} values. The KL loss helps prevent trivial solutions (*e.g.*, collapsing to zero noise) by regularizing the learned noise distribution. Our results indicate that setting $\lambda_{KL} = 1.0$ yields the best performance. Larger values overly bias the model toward the prior, ignoring structure-specific features, while smaller values lead to under-regularized, uninformative noise distributions. Together, these results highlight the importance of carefully balancing prior assumptions and regularization strength when modeling physically meaningful noise.

4.4 Case Study: Validating Anisotropic Noise Behavior on Crystal and Molecular Structures

To verify whether the learned noise captures the physical anisotropy of the energy landscape, we design an experiment to probe how directional perturbations influence energy changes. To quantitatively evaluate this effect, we first perform eigenvalue decomposition on the learned covariance matrices and apply small random perturbations along the resulting eigenvectors. The corresponding changes in energy are then measured using the Symmetric Mean Absolute Percentage Error (sMAPE).

Crystal Validation. The resulting energy changes, along with the associated eigenvectors and eigenvalues, are visualized in Figure 3(c).

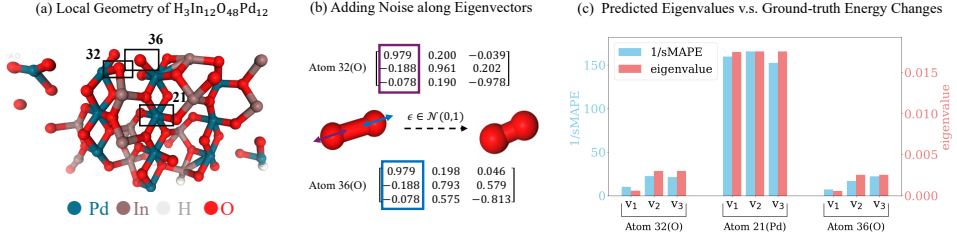


Figure 3: Visualization of the $\text{H}_3\text{In}_{12}\text{O}_{48}\text{Pd}_{12}$ crystal. We select oxygen atoms at indices $\{32, 36\}$, and a palladium atom at index 21. Figure (b) presents the eigenvectors of the oxygens. Figure (c) shows the relationship between the structural energy and applied noise.

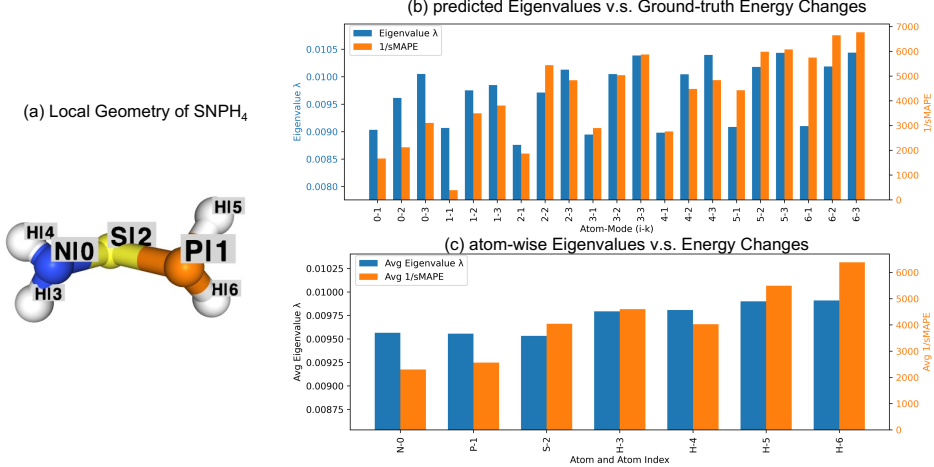


Figure 4: Analysis on the SNPH_4 molecule. (a) Local geometry showing atom indices. (b) Per-atom directional alignment between predicted eigenvalues and ground-truth energy sensitivities (1/sMAPE). (c) Atom-wise comparison of averaged eigenvalues and energy sensitivities.

For example, atoms $\{32, 36\}$ are spatially close, identical oxygen atoms with strong repulsive interaction. **The eigenvector corresponding to the smallest eigenvalue for both atoms aligns with the bond direction between them (Figure 3b).** Due to the short distance and strong repulsion, perturbations along this axis lead to significant energy changes, and AniDS accordingly reduces noise in this direction. In contrast, atom 21 resides in a more symmetric environment. The model thus produces larger and more isotropic noise for this atom. This strongly supports our main idea: AniDS allows for structure-aware noise generation, reducing excessive disruption.

Molecular Validation. To further confirm the generality of the anisotropic noise modeling, we conduct an additional analysis on the SNPH_4 molecule.

Figure 4(b) shows that the predicted eigenvalues exhibit a consistent trend with the ground-truth energy changes measured by 1/sMAPE, demonstrating that AniDS effectively captures direction-dependent energy stiffness. Notably, for atoms H6–1 and H5–1, the smallest eigenvalues correspond to eigenvectors aligned with the two P–H bonds, matching the physically stiff directions of the molecule. Figure 4(c) further summarizes the per-atom averaged behavior. Hydrogen atoms display larger eigenvalues and higher 1/sMAPE values, indicating that their displacements have relatively minor effects on total energy. In contrast, the N, P, and S atoms situated at the core of the molecular structure and show smaller eigenvalues, signifying greater energy sensitivity to positional perturbations. The results show that perturbations along different directions affect the potential energy surface to varying degrees, validating the rationale behind the anisotropic noise design: **AniDS suppresses perturbations in energy-sensitive directions while allowing more noise along flexible axes, closely aligning with the ground-truth energy changes.**

5 Related Works

Coordinate Denoising for 3D Atomistic Systems. Coordinate denoising has been widely explored for pretraining on 3D atomistic systems [12, 13, 31, 17, 22], showing strong performance in predicting

quantum chemical properties, force fields, and energies [44, 45, 18]. While the method was originally proposed to equilibrium molecular structures, it is later extended to non-equilibrium systems by incorporating atomic force information into the model [27]. Coordinate denoising’s effectiveness stems from its theoretical connection to learning molecular force fields [13], under the assumption that the noise distribution is isotropic Gaussian and the data distribution is a mixture of such Gaussians. To overcome the limitations of the isotropic assumption, Frad [17] combines torsional and coordinate noise, while Slide [18] applies independent Gaussian noise on bond lengths, angles, and torsion angles. However, these methods use fixed noise scales, ignoring the variability of energy potentials across distinct structures. Addressing this, DenoiseVAE [16] leverages a Variational Autoencoder [46] to learn atom-wise adaptive noise variances. In contrast, AniDS learns a full covariance matrix for each atom’s noise distribution, enabling the modeling of anisotropic and structure-aware noise.

Other 3D Molecular Pretraining Methods. A representative approach involves directly pretraining on large-scale molecular dynamics simulation datasets. For example, MatterSim [47] and JMP [48] are trained on large-scale molecular dynamics trajectories and achieve strong performance on downstream property prediction tasks. However, these methods rely heavily on high-quality large-scale simulation datasets, which are often expensive to obtain and limited in scalability. Another line of work focuses on integrating multiple structural representations to improve model expressiveness. For instance, MoleculeSDE [49] and Transformer-M [50] combine 2D topological graphs with 3D geometric point clouds, using complementary perspectives to enhance molecular representations. UniCorn [51] unifies three mainstream self-supervised strategies into a multi-view contrastive learning framework to construct more comprehensive molecular representations. MoleBlend [52] fuses 2D and 3D structural information at the atomic relation level, enabling fine-grained structural modeling. Recent advances further explore cross-modal and language-grounded representations for molecular systems. 3D-MoLM [53] and MolCA [54] align molecular graphs and textual descriptions through multimodal pretraining, while NEXT-MOL [55] and ReactXT [56] integrate 3D diffusion or reaction-context modeling with language understanding. SIMSGT [57] revisits tokenization and decoding for masked graph modeling, and ProtT3 [58] extends text-based pretraining to proteins. Beyond molecule-text alignment, UAE-3D [59] propose a unified latent space for 3D molecular diffusion, and scMMGPT [60] leverage language models for single-cell representation learning. At a broader scale, NatureLM [61] envisions a general language of natural sciences, and deep-learning frameworks such as [62] highlight the potential of AI to uncover physical principles in crystalline materials.

6 Conclusion and Future Work

We present AniDS, a denoising framework that learns anisotropic, structure-aware noise distributions to enhance molecular force field modeling. By generating atom-specific full covariance matrices conditioned on molecular geometry, AniDS lifts the isotropic and homoscedastic assumptions inherent in prior denoising methods. Grounded in theoretical connections to force field learning, AniDS supports both pretraining and auxiliary fine-tuning. Extensive experiments on MD17 and OC22 show that AniDS achieves leading performance. Looking forward, we aim to extend AniDS to larger and more complex systems, such as proteins and RNAs, and apply it for molecular simulations.

7 Acknowledgement

This work was supported in part by the Ministry of Education (MOE T1251RES2309 and MOE T2EP20125-0039) and the Agency for Science, Technology and Research (A*STAR H25J6a0034).

References

- [1] Alexandre Blanco-Gonzalez, Alfonso Cabezon, Alejandro Seco-Gonzalez, Daniel Conde-Torres, Paula Antelo-Riveiro, Angel Pineiro, and Rebeca Garcia-Fandino. The role of ai in drug discovery: challenges, opportunities, and strategies. *Pharmaceuticals*, 16(6):891, 2023.
- [2] Kit-Kay Mak, Yi-Hang Wong, and Mallikarjuna Rao Pichika. Artificial intelligence in drug discovery and development. *Drug discovery and evaluation: safety and pharmacokinetic assays*, pages 1461–1498, 2024.
- [3] Dana Bishara, Yuxi Xie, Wing Kam Liu, and Shaofan Li. A state-of-the-art review on machine learning-based multiscale modeling, simulation, homogenization and design of materials. *Archives of computational methods in engineering*, 30(1):191–222, 2023.

[4] Lowik Chanussot, Abhishek Das, Siddharth Goyal, Thibaut Lavril, Muhammed Shuaibi, Morgane Riviere, Kevin Tran, Javier Heras-Domingo, Caleb Ho, Weihua Hu, et al. Open catalyst 2020 (oc20) dataset and community challenges. *Acs Catalysis*, 11(10):6059–6072, 2021.

[5] Janice Lan, Aini Palizhati, Muhammed Shuaibi, Brandon M Wood, Brook Wander, Abhishek Das, Matt Uyttendaele, C Lawrence Zitnick, and Zachary W Ulissi. Adsorbm: a leap in efficiency for adsorption energy calculations using generalizable machine learning potentials. *npj Computational Materials*, 9(1):172, 2023.

[6] Boris Kozinsky, Albert Musaelian, Anders Johansson, and Simon Batzner. Scaling the leading accuracy of deep equivariant models to biomolecular simulations of realistic size. In *Proceedings of the International Conference for High Performance Computing, Networking, Storage and Analysis*, pages 1–12, 2023.

[7] Stefan Chmiela, Alexandre Tkatchenko, Huziel E Sauceda, Igor Poltavsky, Kristof T Schütt, and Klaus-Robert Müller. Machine learning of accurate energy-conserving molecular force fields. *Science advances*, 3(5):e1603015, 2017.

[8] Robert G. Parr and Weitao Yang. *Density-Functional Theory of Atoms and Molecules*. Oxford University Press, USA, 1994.

[9] Jörg Behler. Perspective: Machine learning potentials for atomistic simulations. *The Journal of chemical physics*, 145(17), 2016.

[10] Simon Batzner, Albert Musaelian, Lixin Sun, Mario Geiger, Jonathan P Mailoa, Mordechai Kornbluth, Nicola Molinari, Tess E Smidt, and Boris Kozinsky. E(3)-equivariant graph neural networks for data-efficient and accurate interatomic potentials. *Nature communications*, 13(1):2453, 2022.

[11] Oliver Unke, Mihail Bogojeski, Michael Gastegger, Mario Geiger, Tess Smidt, and Klaus-Robert Müller. Se(3)-equivariant prediction of molecular wavefunctions and electronic densities. *Advances in Neural Information Processing Systems*, 34:14434–14447, 2021.

[12] Jonathan Godwin, Michael Schaarschmidt, Alexander Gaunt, Alvaro Sanchez-Gonzalez, Yulia Rubanova, Petar Veličković, James Kirkpatrick, and Peter Battaglia. Simple gnn regularisation for 3d molecular property prediction & beyond. *arXiv preprint arXiv:2106.07971*, 2021.

[13] Sheheryar Zaidi, Michael Schaarschmidt, James Martens, Hyunjik Kim, Yee Whye Teh, Alvaro Sanchez-Gonzalez, Peter Battaglia, Razvan Pascanu, and Jonathan Godwin. Pre-training via denoising for molecular property prediction. *arXiv preprint arXiv:2206.00133*, 2022.

[14] Andrew R Leach. *Molecular modelling: principles and applications*. Pearson education, 2001.

[15] Trevor Hastie, Robert Tibshirani, Jerome H Friedman, and Jerome H Friedman. *The elements of statistical learning: data mining, inference, and prediction*, volume 2. Springer, 2009.

[16] Yurou Liu, Jiahao Chen, Rui Jiao, Jiangmeng Li, Wenbing Huang, and Bing Su. Denoisevae: Learning molecule-adaptive noise distributions for denoising-based 3d molecular pre-training. In *The Thirteenth International Conference on Learning Representations*, 2025.

[17] Shikun Feng, Yuyan Ni, Yanyan Lan, Zhi-Ming Ma, and Wei-Ying Ma. Fractional denoising for 3d molecular pre-training. In *International Conference on Machine Learning*, pages 9938–9961. PMLR, 2023.

[18] Yuyan Ni, Shikun Feng, Wei-Ying Ma, Zhi-Ming Ma, and Yanyan Lan. Sliced denoising: A physics-informed molecular pre-training method. *arXiv preprint arXiv:2311.02124*, 2023.

[19] Kaiming He, Xinlei Chen, Saining Xie, Yanghao Li, Piotr Dollár, and Ross Girshick. Masked autoencoders are scalable vision learners. In *Proceedings of the IEEE/CVF conference on computer vision and pattern recognition*, pages 16000–16009, 2022.

[20] Jacob Devlin, Ming-Wei Chang, Kenton Lee, and Kristina Toutanova. Bert: Pre-training of deep bidirectional transformers for language understanding. In *Proceedings of the 2019 conference of the North American chapter of the association for computational linguistics: human language technologies, volume 1 (long and short papers)*, pages 4171–4186, 2019.

[21] Zhiyuan Liu, Yaorui Shi, An Zhang, Enzhi Zhang, Kenji Kawaguchi, Xiang Wang, and Tat-Seng Chua. Rethinking tokenizer and decoder in masked graph modeling for molecules. *Advances in Neural Information Processing Systems*, 36:25854–25875, 2023.

[22] Yuyang Wang, Changwen Xu, Zijie Li, and Amir Barati Farimani. Denoise pretraining on nonequilibrium molecules for accurate and transferable neural potentials. *Journal of Chemical Theory and Computation*, 19(15):5077–5087, 2023.

[23] Tianlang Chen, Shengjie Luo, Di He, Shuxin Zheng, Tie-Yan Liu, and Liwei Wang. Geomformer: A general architecture for geometric molecular representation learning. *arXiv preprint arXiv:2406.16853*, 2024.

[24] Yi-Lun Liao, Brandon Wood, Abhishek Das, and Tess Smidt. Equiformer2: Improved equivariant transformer for scaling to higher-degree representations. In *ICLR*, 2024.

[25] Gene H Golub and Charles F Van Loan. *Matrix computations*. JHU press, 2013.

[26] Yusong Wang, Shaoning Li, Tong Wang, Bin Shao, Nanning Zheng, and Tie-Yan Liu. Geometric transformer with interatomic positional encoding. *Advances in Neural Information Processing Systems*, 36:55981–55994, 2023.

[27] Yi-Lun Liao, Tess Smidt, Muhammed Shuaibi, and Abhishek Das. Generalizing denoising to non-equilibrium structures improves equivariant force fields. *arXiv preprint arXiv:2403.09549*, 2024.

[28] Johannes Gasteiger, Janek Groß, and Stephan Günnemann. Directional message passing for molecular graphs. *arXiv preprint arXiv:2003.03123*, 2020.

[29] Yang Song and Stefano Ermon. Generative modeling by estimating gradients of the data distribution. *Advances in neural information processing systems*, 32, 2019.

[30] Pascal Vincent. A connection between score matching and denoising autoencoders. *Neural computation*, 23(7):1661–1674, 2011.

[31] Shengchao Liu, Hongyu Guo, and Jian Tang. Molecular geometry pretraining with se (3)-invariant denoising distance matching. *arXiv preprint arXiv:2206.13602*, 2022.

[32] Maho Nakata and Tomomi Shimazaki. Pubchemqc project: a large-scale first-principles electronic structure database for data-driven chemistry. *Journal of chemical information and modeling*, 57(6):1300–1308, 2017.

[33] Richard Tran, Janice Lan, Muhammed Shuaibi, Brandon M Wood, Siddharth Goyal, Abhishek Das, Javier Heras-Domingo, Adeesh Kolluru, Ammar Rizvi, Nima Shoghi, et al. The open catalyst 2022 (oc22) dataset and challenges for oxide electrocatalysts. *ACS Catalysis*, 13(5):3066–3084, 2023.

[34] Stefan Chmiela, Alexandre Tkatchenko, Huziel E Sauceda, Igor Poltavsky, Kristof T Schütt, and Klaus-Robert Müller. Machine learning of accurate energy-conserving molecular force fields. *Science advances*, 3(5):e1603015, 2017.

[35] Bowen Deng, Peichen Zhong, KyuJung Jun, Janosh Riebesell, Kevin Han, Christopher J Bartel, and Gerbrand Ceder. Chgnet as a pretrained universal neural network potential for charge-informed atomistic modelling. *Nature Machine Intelligence*, 5(9):1031–1041, 2023.

[36] Anubhav Jain, Shyue Ping Ong, Geoffroy Hautier, Wei Chen, William Davidson Richards, Stephen Dacek, Shreyas Cholia, Dan Gunter, David Skinner, Gerbrand Ceder, and Kristin A. Persson. Commentary: The materials project: A materials genome approach to accelerating materials innovation. *APL Materials*, 1(1):011002, 07 2013.

[37] Kristof T Schütt, Huziel E Sauceda, P-J Kindermans, Alexandre Tkatchenko, and K-R Müller. Schnet—a deep learning architecture for molecules and materials. *The Journal of Chemical Physics*, 148(24), 2018.

[38] Johannes Gasteiger, Shankari Giri, Johannes T Margraf, and Stephan Günnemann. Fast and uncertainty-aware directional message passing for non-equilibrium molecules. *arXiv preprint arXiv:2011.14115*, 2020.

[39] Kristof Schütt, Oliver Unke, and Michael Gastegger. Equivariant message passing for the prediction of tensorial properties and molecular spectra. In *International Conference on Machine Learning*, pages 9377–9388. PMLR, 2021.

[40] Philipp Thölke and Gianni De Fabritiis. Torchmd-net: equivariant transformers for neural network based molecular potentials. *arXiv preprint arXiv:2202.02541*, 2022.

[41] Shengchao Liu, Hongyu Guo, and Jian Tang. Molecular geometry pretraining with SE(3)-invariant denoising distance matching. In *The Eleventh International Conference on Learning Representations*, 2023.

[42] Johannes Gasteiger, Muhammed Shuaibi, Anuroop Sriram, Stephan Günnemann, Zachary Ulissi, C Lawrence Zitnick, and Abhishek Das. Gemnet-oc: developing graph neural networks for large and diverse molecular simulation datasets. *arXiv preprint arXiv:2204.02782*, 2022.

[43] Yunyang Li, Lin Huang, Zhihao Ding, Chu Wang, Xinran Wei, Han Yang, Zun Wang, Chang Liu, Yu Shi, Peiran Jin, et al. E2former: A linear-time efficient and equivariant transformer for scalable molecular modeling. *arXiv e-prints*, pages arXiv–2501, 2025.

[44] Rui Jiao, Jiaqi Han, Wenbing Huang, Yu Rong, and Yang Liu. Energy-motivated equivariant pretraining for 3d molecular graphs. In *Proceedings of the AAAI Conference on Artificial Intelligence*, volume 37, pages 8096–8104, 2023.

[45] Gengmo Zhou, Zhifeng Gao, Qiankun Ding, Hang Zheng, Hongteng Xu, Zhewei Wei, Linfeng Zhang, and Guolin Ke. Uni-mol: A universal 3d molecular representation learning framework. 2023.

[46] Diederik P. Kingma and Max Welling. Auto-encoding variational bayes. In *ICLR*, 2014.

[47] Han Yang, Chenxi Hu, Yichi Zhou, Xixian Liu, Yu Shi, Jielan Li, Guanzhi Li, Zekun Chen, Shuizhou Chen, Claudio Zeni, et al. Mattersim: A deep learning atomistic model across elements, temperatures and pressures. *arXiv preprint arXiv:2405.04967*, 2024.

[48] Nima Shoghi, Adeesh Kolluru, John R Kitchin, Zachary W Ulissi, C Lawrence Zitnick, and Brandon M Wood. From molecules to materials: Pre-training large generalizable models for atomic property prediction. *arXiv preprint arXiv:2310.16802*, 2023.

[49] Shengchao Liu, Weitao Du, Zhi-Ming Ma, Hongyu Guo, and Jian Tang. A group symmetric stochastic differential equation model for molecule multi-modal pretraining. In *International Conference on Machine Learning*, pages 21497–21526. PMLR, 2023.

[50] Shengjie Luo, Tianlang Chen, Yixian Xu, Shuxin Zheng, Tie-Yan Liu, Liwei Wang, and Di He. One transformer can understand both 2d & 3d molecular data. *arXiv preprint arXiv:2210.01765*, 2022.

[51] Shikun Feng, Yuyan Ni, Minghao Li, Yanwen Huang, Zhi-Ming Ma, Wei-Ying Ma, and Yanyan Lan. Unicorn: A unified contrastive learning approach for multi-view molecular representation learning. *arXiv preprint arXiv:2405.10343*, 2024.

[52] Qiying Yu, Yudi Zhang, Yuyan Ni, Shikun Feng, Yanyan Lan, Hao Zhou, and Jingjing Liu. Multimodal molecular pretraining via modality blending. *arXiv preprint arXiv:2307.06235*, 2023.

[53] Sihang Li, Zhiyuan Liu, Yanchen Luo, Xiang Wang, Xiangnan He, Kenji Kawaguchi, Tat-Seng Chua, and Qi Tian. 3d-molm: Towards 3d molecule-text interpretation in language models. In *ICLR*, 2024.

[54] Zhiyuan Liu, Sihang Li, Yanchen Luo, Hao Fei, Yixin Cao, Kenji Kawaguchi, Xiang Wang, and Tat-Seng Chua. Molca: Molecular graph-language modeling with cross-modal projector and uni-modal adapter. In *EMNLP*, 2023.

[55] Zhiyuan Liu, Yanchen Luo, Han Huang, Enzhi Zhang, Sihang Li, Junfeng Fang, Yaorui Shi, Xiang Wang, Kenji Kawaguchi, and Tat-Seng Chua. NEXT-MOL: 3d diffusion meets 1d language modeling for 3d molecule generation. In *The Thirteenth International Conference on Learning Representations*, 2025.

[56] Zhiyuan Liu, Yaorui Shi, An Zhang, Sihang Li, Enzhi Zhang, Xiang Wang, Kenji Kawaguchi, and Tat-Seng Chua. Reactxt: Understanding molecular “reaction-ship” via reaction-contextualized molecule-text pretraining. In *Findings of the Association for Computational Linguistics: ACL 2024*. Association for Computational Linguistics, 2024.

[57] Zhiyuan Liu, Yaorui Shi, An Zhang, Enzhi Zhang, Kenji Kawaguchi, Xiang Wang, and Tat-Seng Chua. Rethinking tokenizer and decoder in masked graph modeling for molecules. In *NeurIPS*, 2023.

[58] Zhiyuan Liu, An Zhang, Hao Fei, Enzhi Zhang, Xiang Wang, Kenji Kawaguchi, and Tat-Seng Chua. Prott3: Protein-to-text generation for text-based protein understanding. In *ACL*. Association for Computational Linguistics, 2024.

[59] Yanchen Luo, Zhiyuan Liu, Yi Zhao, Sihang Li, Hengxing Cai, Kenji Kawaguchi, Tat-Seng Chua, Yang Zhang, and Xiang Wang. Towards unified and lossless latent space for 3d molecular latent diffusion modeling. *arXiv preprint arXiv:2503.15567*, 2025.

[60] Yaorui Shi, Jiaqi Yang, Changhao Nai, Sihang Li, Junfeng Fang, Xiang Wang, Zhiyuan Liu, and Yang Zhang. Language-enhanced representation learning for single-cell transcriptomics. *arXiv preprint arXiv:2503.09427*, 2025.

[61] Yingce Xia, Peiran Jin, Shufang Xie, Liang He, Chuan Cao, Renqian Luo, Guoqing Liu, Yue Wang, Zequn Liu, Yuan-Jyue Chen, et al. Naturelm: Deciphering the language of nature for scientific discovery. *arXiv e-prints*, pages arXiv–2502, 2025.

[62] Jielan Li, Zekun Chen, Qian Wang, Han Yang, Ziheng Lu, Guanzhi Li, Shuizhou Chen, Yu Zhu, Xianxian Liu, Junfu Tan, et al. Probing the limit of heat transfer in inorganic crystals with deep learning. *arXiv preprint arXiv:2503.11568*, 2025.

[63] Jonathan Schmidt, Tiago FT Cerqueira, Aldo H Romero, Antoine Loew, Fabian Jäger, Hai-Chen Wang, Silvana Botti, and Miguel AL Marques. Improving machine-learning models in materials science through large datasets. *Materials Today Physics*, 48:101560, 2024.

[64] Jinzhe Zeng, Duo Zhang, Anyang Peng, Xiangyu Zhang, Sensen He, Yan Wang, Xinzijian Liu, Hangrui Bi, Yifan Li, Chun Cai, et al. Deepmd-kit v3: A multiple-backend framework for machine learning potentials. *Journal of Chemical Theory and Computation*, 2025.

[65] Ilyes Batatia, David P Kovacs, Gregor Simm, Christoph Ortner, and Gábor Csányi. Mace: Higher order equivariant message passing neural networks for fast and accurate force fields. *Advances in neural information processing systems*, 35:11423–11436, 2022.

[66] Luis Barroso-Luque, Muhammed Shuaibi, Xiang Fu, Brandon M Wood, Misko Dzamba, Meng Gao, Ammar Rizvi, C Lawrence Zitnick, and Zachary W Ulissi. Open materials 2024 (omat24) inorganic materials dataset and models. *arXiv preprint arXiv:2410.12771*, 2024.

[67] Viktor Zaverkin, Francesco Alesiani, Takashi Maruyama, Federico Errica, Henrik Christiansen, Makoto Takamoto, Nicolas Weber, and Mathias Niepert. Higher-rank irreducible cartesian tensors for equivariant message passing. *Advances in Neural Information Processing Systems*, 37:124025–124068, 2024.

- [68] Anders S Christensen and O Anatole Von Lilienfeld. On the role of gradients for machine learning of molecular energies and forces. *Machine Learning: Science and Technology*, 1(4):045018, 2020.
- [69] Stefan Chmiela, Valentin Vassilev-Galindo, Oliver T Unke, Adil Kabylda, Huziel E Sauceda, Alexandre Tkatchenko, and Klaus-Robert Müller. Accurate global machine learning force fields for molecules with hundreds of atoms. *Science Advances*, 9(2):eadf0873, 2023.
- [70] Yunyang Li, Yusong Wang, Lin Huang, Han Yang, Xinran Wei, Jia Zhang, Tong Wang, Zun Wang, Bin Shao, and Tie-Yan Liu. Long-short-range message-passing: A physics-informed framework to capture non-local interaction for scalable molecular dynamics simulation. *arXiv preprint arXiv:2304.13542*, 2023.

A Limitations

Coupled Atomic Motions. Atomic motions are coupled. For example, the stretch-bend coupling is a well-known effect where the stretching of a bond can influence the angle between adjacent atoms. While AniDS models anisotropic noise at the per-atom level with pairwise directional corrections, it does not explicitly capture higher-order couplings among three or more atoms. This may limit its ability to fully represent complex correlated motions, such as torsional barriers or cooperative vibrations in larger systems. Future work could explore incorporating multi-body structural priors or higher-order interaction terms into the noise generator to better reflect these coupling effects.

Approximated Force Field Modeling. Similar to prior works [17, 27], the proposed AniDS framework approximates force field learning by modeling the noise distribution. To achieve high-accuracy predictions, it should be paired with supervised force learning—either during fine-tuning or joint training. The role of AniDS is to enhance the effectiveness of supervised force field learning by providing a more informative and physically grounded initialization, or act as a regularization.

B More Details on Methodology

B.1 The Backbones of Denoising Auto-encoder and Force Encoding

EquiformerV2 [24] is an improved SE(3)/E(3)-equivariant Transformer architecture designed to scale to higher-degree representations in 3D atomistic systems. Building upon the original Equiformer, EquiformerV2 replaces computationally expensive SO(3) convolutions with efficient eSCN convolutions based on SO(2) operations, reducing the computational complexity from $\mathcal{O}(L_{\max}^6)$ to $\mathcal{O}(L_{\max}^3)$. To further leverage higher-order equivariant features, it introduces three architectural innovations: *attention re-normalization*, *separable S^2 activation*, and *separable layer normalization*. These enhancements improve model expressivity, data efficiency, and numerical stability. EquiformerV2 achieves leading performances on large-scale datasets such as OC20 and OC22 for energy and force prediction, demonstrating strong accuracy over previous equivariant GNNs.

GeoMFormer [23] is a general Transformer-based architecture for geometric molecular representation learning that simultaneously models both invariant and equivariant properties of molecular systems. It employs a dual-stream design: one stream learns invariant features (e.g., energy-related properties), while the other learns equivariant features (e.g., forces or atomic positions). These two streams are connected via carefully designed cross-attention modules, allowing mutual information exchange and enhancing representation quality. This modular design enables GeoMFormer to flexibly incorporate geometric constraints (e.g., SE(3) invariance/equivariance) and supports strong performance across diverse tasks, including energy prediction and molecular dynamics.

Force Encoding. Following [27], in implementation, for the equivariant network of EquiformerV2 [24], we include the additional node-level features of:

$$EM_{\mathbf{f}_i} = SO3_{\text{linear}}(\|\mathbf{f}_i\| \cdot Y\left(\frac{\mathbf{f}_i}{\|\mathbf{f}_i\|}\right)) \quad (22)$$

For the invariant network of GeoMFormer [23], we have additional edge-level features of:

$$EM_{\mathbf{f}_{ij}} = \text{linear}(\mathbf{f}_i \cdot \frac{\mathbf{r}_{ij}}{\|\mathbf{r}_{ij}\|}) \cdot \|\mathbf{r}_{ij}\|. \quad (23)$$

B.2 Proof for the Covariance Matrix’s Properties

Proof that the covariance matrix is positive definite.

Proof. For any non-zero vector $\mathbf{v} \in \mathbb{R}^3$, we compute:

$$\mathbf{v}^\top \Sigma_i \mathbf{v} = a_i \mathbf{v}^\top \mathbf{I} \mathbf{v} - a_i \sum_j \gamma_{ij} \mathbf{v}^\top \left(\frac{\mathbf{r}_{ij} \mathbf{r}_{ij}^\top}{\|\mathbf{r}_{ij}\|^2} \right) \mathbf{v}.$$

Step 1: Simplify Each Term.

1. Isotropic Term:

$$a_i \mathbf{v}^\top \mathbf{I} \mathbf{v} = a_i \|\mathbf{v}\|^2.$$

2. Anisotropic Term:

$$\mathbf{v}^\top \left(\frac{\mathbf{r}_{ij} \mathbf{r}_{ij}^\top}{|\mathbf{r}_{ij}|^2} \right) \mathbf{v} = \left(\frac{\mathbf{v}^\top \mathbf{r}_{ij}}{|\mathbf{r}_{ij}|} \right)^2 = \left(\mathbf{v}^\top \frac{\mathbf{r}_{ij}}{|\mathbf{r}_{ij}|} \right)^2 = (\mathbf{v} \cdot \mathbf{u}_{ij})^2,$$

where $\mathbf{u}_{ij} = \mathbf{r}_{ij}/|\mathbf{r}_{ij}|$ is a unit vector.

Step 2: Combine Terms. Substitute back into $\mathbf{v}^\top \Sigma_i \mathbf{v}$:

$$\mathbf{v}^\top \Sigma_i \mathbf{v} = a_i \|\mathbf{v}\|^2 - a_i \sum_j \gamma_{ij} (\mathbf{v} \cdot \mathbf{u}_{ij})^2.$$

Factor out $a_i > 0$:

$$= a_i \left(\|\mathbf{v}\|^2 - \sum_j \gamma_{ij} (\mathbf{v} \cdot \mathbf{u}_{ij})^2 \right).$$

Step 3: Bounding the Anisotropic Correction. The term $\sum_j \gamma_{ij} (\mathbf{v} \cdot \mathbf{u}_{ij})^2$ represents the weighted sum of squared projections of \mathbf{v} onto the directions \mathbf{u}_{ij} . By the Cauchy-Schwarz inequality:

$$(\mathbf{v} \cdot \mathbf{u}_{ij})^2 \leq \|\mathbf{v}\|^2 \|\mathbf{u}_{ij}\|^2 = \|\mathbf{v}\|^2.$$

Thus:

$$\sum_j \gamma_{ij} (\mathbf{v} \cdot \mathbf{u}_{ij})^2 \leq \sum_j \gamma_{ij} \|\mathbf{v}\|^2 = \|\mathbf{v}\|^2 \sum_j \gamma_{ij}.$$

Step 4: Ensuring Positivity. From Equation (9), the normalization ensures:

$$\sum_j \gamma_{ij} = \frac{\sum_j \exp(b_{ij})}{\sum_j \exp(b_{ij}) + c_i} < 1,$$

since $c_i = \exp(\omega_2(\mathbf{h}_i)) > 0$. Therefore:

$$\|\mathbf{v}\|^2 - \sum_j \gamma_{ij} (\mathbf{v} \cdot \mathbf{u}_{ij})^2 \geq \|\mathbf{v}\|^2 - \|\mathbf{v}\|^2 \sum_j \gamma_{ij} = \|\mathbf{v}\|^2 (1 - \sum_j \gamma_{ij}) > 0.$$

Step 5: Final Result. Since $a_i > 0$ and the bracketed term is positive:

$$\mathbf{v}^\top \Sigma_i \mathbf{v} = a_i \cdot (\text{positive term}) > 0.$$

Thus, Σ_i is positive definite. \square

B.3 Detailed Method for Applying AniDS with Partially Corrupted Material Structures

Specifically, for a material \mathbf{M} , we first stochastically decide whether to apply noise perturbation with probability p_{DeNS} . If applied, we perturb only a subset of atoms with the fraction r_{DeNS} . This separates the material into two subsets: the *perturbed atoms* \mathbf{M}_{pert} and the *unperturbed atoms* $\mathbf{M}_{\text{unpert}}$. For the perturbed atoms, the atomic-level forces $\mathbf{F}_{\text{pert}} \in \mathbb{R}^{N_{\text{pert}} \times 3}$ are explicitly encoded as model inputs, and they are optimized using the AniDS loss. For the unperturbed atoms, we do not use atomic-level forces $\mathbf{F}_{\text{unpert}} \in \mathbb{R}^{(N - N_{\text{pert}}) \times 3}$ as input, but use it to train the model. This design ensures the model learns to infer forces on unperturbed regions from contextual information, while leveraging explicit force signals from perturbed regions to guide denoising.

The denoising module ψ consumes the partially perturbed structure $\tilde{\mathbf{M}}$ and produces several outputs: (1) atom-wise noise predictions $\omega_{\hat{\epsilon}} \circ \psi(\tilde{\mathbf{M}}, \mathbf{F}(\mathbf{M}))$, (2) a global energy prediction $\omega_{\hat{E}} \circ \psi(\tilde{\mathbf{M}}, \mathbf{F}(\mathbf{M}))$, (3) atom-wise force predictions $\omega_{\hat{f}} \circ \psi(\tilde{\mathbf{M}}, \mathbf{F}(\mathbf{M})) = \{\hat{f}_i \in \mathbb{R}^3 \mid i \in \mathbf{M}\}$, and (4) a stress tensor

prediction $\omega_{\hat{\rho}} \circ \psi(\tilde{\mathbf{M}}, \mathbf{F}(\mathbf{M}))$. $\omega_{\hat{\epsilon}}$, $\omega_{\hat{f}}$, and $\omega_{\hat{E}}$ are prediction heads, depending on the used backbone molecular denoising autoencoder. The loss functions for these properties are defined as follows:

$$\mathcal{L}_E = \mathbb{E}_{q_{\Sigma}(\tilde{\mathbf{X}}, \mathbf{X})} \|E(\mathbf{M}) - \hat{E}(\tilde{\mathbf{M}}, \mathbf{F}(\mathbf{M}))\|, \quad (24)$$

$$\mathcal{L}_F = \frac{1}{|\mathbf{M}_{\text{unpert}}|} \mathbb{E}_{q_{\Sigma}(\tilde{\mathbf{X}}, \mathbf{X})} \sum_{i \in \mathbf{M}_{\text{unpert}}} \|f_i(\mathbf{M}) - \hat{f}_i(\tilde{\mathbf{M}}, \mathbf{F}(\mathbf{M}))\|^2, \quad (25)$$

$$\mathcal{L}_{\rho} = \mathbb{E}_{q_{\Sigma}(\tilde{\mathbf{X}}, \mathbf{X})} \|\rho(\mathbf{M}) - \hat{\rho}(\tilde{\mathbf{M}}, \mathbf{F}(\mathbf{M}))\|, \quad (26)$$

The overall loss of this formulation is:

$$\mathcal{L} = \lambda_E \mathcal{L}_E + \lambda_F \mathcal{L}_F + \lambda_{\rho} \mathcal{L}_{\rho} + \lambda_{\text{AniDS}} \mathcal{L}_{\text{AniDS}} + \lambda_{\text{KL}} \mathcal{L}_{\text{KL}} + \lambda_{\gamma} \mathcal{L}_{\gamma}, \quad (27)$$

where the AniDS and KL loss are only computed for the perturbed atoms.

B.4 Proof of that DenoiseVAE and DeNS are Special Cases of AniDS

Proof. DenoiseVAE as a Special Case of AniDS.

To demonstrate that DenoiseVAE is a special case of the AniDS framework, we show that AniDS reduces to DenoiseVAE under the following constraints:

Step 1. Restriction to Diagonal Covariance Matrices. In AniDS, the noise generator produces a full covariance matrix $\Sigma_i \in \mathbb{R}^{3 \times 3}$ for each atom i . DenoiseVAE, however, assumes isotropic noise with diagonal covariance:

$$\Sigma_i = \sigma_i^2 \mathbf{I},$$

where $\sigma_i \in \mathbb{R}^+$ is a scalar variance. This reduces the anisotropic noise in AniDS to isotropic noise, ignoring directional correlations.

Step 2. Alignment of Denoising Objectives. The denoising loss in AniDS (Equation (9)) becomes equivalent to DenoiseVAE’s loss under diagonal covariance:

$$\mathcal{L}_{\text{AniDS}} = \mathbb{E} \sum_{i=1}^N \left\| \phi(\tilde{\mathbf{M}})_i - \Sigma_i^{-1} (\tilde{\mathbf{X}}_i - \mathbf{X}_i) \right\|^2.$$

For $\Sigma_i = \sigma_i^2 \mathbf{I}$, the inverse $\Sigma_i^{-1} = \frac{1}{\sigma_i^2} \mathbf{I}$, leading to:

$$\mathcal{L}_{\text{AniDS}} = \mathbb{E} \sum_{i=1}^N \sigma_i^2 \left\| \phi(\tilde{\mathbf{M}})_i - \frac{\tilde{\mathbf{X}}_i - \mathbf{X}_i}{\sigma_i^2} \right\|^2,$$

which matches DenoiseVAE’s loss $\mathcal{L}_{\text{Denoise}}$ (Equation 3 in the paper).

Step 3. Noise Generation and Training Paradigm. AniDS: Jointly trains a noise generator (for Σ_i) and a denoising autoencoder ϕ . DenoiseVAE: Jointly trains a noise generator (for σ_i^2) and a denoising module \mathcal{D}_{θ} , following a VAE framework. When Σ_i is diagonal, AniDS’s noise generator simplifies to DenoiseVAE’s variance predictor, and both use the same variational training strategy.

Conclusion. By constraining AniDS’s covariance matrices Σ_i to be isotropic ($\Sigma_i = \sigma_i^2 \mathbf{I}$), the framework exactly recovers DenoiseVAE. This makes DenoiseVAE a diagonal-covariance special case of the more general AniDS framework, which supports full anisotropic noise distributions. \square

DeNS [27] can also be viewed as a special case of AniDS. Specifically, it corresponds to the setting where the noise covariance Σ_i is fixed and shared across all atoms, *i.e.*, $\Sigma_i = \sigma^2 \mathbf{I}$ for a constant scalar σ . Unlike DenoiseVAE, which learns σ_i per atom, DeNS applies a uniform and non-trainable isotropic noise. The derivation follows the same structure as above and can be obtained by applying this additional constraint to the AniDS framework.

Table 4: MAE comparison between models trained on MPTrj and tested on the ALEXANDRIA set.

Model	Params	Energy (eV)	Force (eV/Å)	Stress (eV/Å ³)
DPA3-v2-MPTrj [64]	4.92M	0.2738	0.0207	0.0035
MACE-MP-0 [65]	4.69M	0.4939	0.0256	0.0046
EquiformerV2 + DeNS [66]	31M	0.2729	0.0134	0.0018
GeoMFormer + AniDS	3M	0.3030	0.0211	—
EquiformerV2 + AniDS (ours)	34M	0.2679 ^{+1.83%}	0.0124 ^{+7.5%}	0.0016 ^{+11.1%}

C More Experimental Results

C.1 Results on MPTrj

Following a similar experimental setup as in Section 4.2, we perform supervised learning with partial corruption and auxiliary denoising on the MPTrj dataset. For evaluation, we use a part of the ALEXANDRIA dataset [63](random 15k structures) as the test set instead of MPTrj’s own split, since prior works adopt different data partitions for MPTrj. This approach helps avoid potential data leakage across models and ensures a fair comparison.

As shown in Table 4, our proposed AniDS framework outperforms baselines on all of three tasks. These results highlight the effectiveness of AniDS in improving force field modeling across diverse evaluation settings.

C.2 More Experimental Settings

C.2.1 Pre-training and Fine-tuning

Pre-training setup. We trained the Equiformer-V2 model on PCQM4Mv2. Our code implementation is based on the repository provided by DeNS [27]. We provide comprehensive training parameters in Table 5. The model was trained on 4 NVIDIA A100 GPUs(40G) and required 32 GPU-hours. The pseudocode for pre-training can be found in Algorithm 1.

Table 5: Hyper-parameters for PCQM4Mv2 pretrain.

Hyper-parameters	Value or description
Optimizer	AdamW
Learning rate scheduling	Cosine
Warmup steps	4000
Maximum learning rate	4×10^{-4}
Batch size (per GPU)	40
Number of steps	40000
Weight decay	0.0
Noise Generator layer	2
Prior distribution σ_p	0.1
KL loss coefficient λ_{kl}	1.0
Regularizer weight λ_γ	1.0

Finetune setup For fine-tuning on MD17, we utilized the code and hyperparameters provided by DeNS [27], specifically as detailed in Table 8. Each task was trained on a single NVIDIA V100 GPU (32GB), with the average running speed per task being similar to that of DeNS. The fine-tuning training procedure is similar to "Supervised Learning with Partial Corruption and Auxiliary Denoising," with the key difference being that during fine-tuning, we no longer train the noise generator (i.e., its associated parameters are frozen). The pseudocode for this training process is similar to that presented in Algorithm 2.

To further assess the robustness of AniDS under more challenging scenarios, we adopted the evaluation protocol established in prior works such as NequIP [10], MACE [65], and ICTP [67]. We conducted experiments on four subsets of the revised MD17 (rMD17) dataset [68] and one subset of the MD22 dataset [69]. The results are presented in Tables 6 and 7.

Table 6: Force MAE (meV/Å) on rMD17 datasets. Lower is better.

Model	Aspirin	Benzene	Toluene	Uracil
NequIP [10]	52.0	2.9	15.1	40.1
MACE [65]	43.9	2.7	12.1	25.9
ICTP [67]	40.19	2.45	11.24	25.97
EquiformerV2	71.40	3.92	19.28	50.45
EquiformerV2 + DeNS	45.52	2.28	11.37	34.46
EquiformerV2 + AniDS (Ours)	40.21	2.31	10.7	28.8

Table 7: Performance comparison on the AT–AT–CG–CG dataset.

Dataset	ICTP [67]	ViSNet-LSRM [70]	MACE [65]	Allegro [70]	TorchMD-Net [70]	sGDML[69]	Equiformer [70]	Equiformer + AniDS (Ours)
AT–AT–CG–CG	3.37	4.61	5.00	5.55	14.13	30.36	5.43	3.22

For each molecule in rMD17, we used 50 training samples, following the ICTP configuration. Both pretraining and fine-tuning employed the $l_{\max} = 3$ variant of EquiformerV2. The hyperparameters used for fine-tuning are summarized in Table 9.

Table 8: Hyper-parameters for fine-tuning on MD17 dataset.

Hyper-parameter	Aspirin	Benzene	Ethanol	Malonaldehyde	Naphthalene	Salicylic acid	Toluene	Uracil
Optimizer	AdamW	AdamW	AdamW	AdamW	AdamW	AdamW	AdamW	AdamW
Learning rate scheduling	Cosine	Cosine	Cosine	Cosine	Cosine	Cosine	Cosine	Cosine
Warm epochs	10	10	10	10	10	10	10	10
Weight decay	1e-6	1e-6	1e-6	1e-6	1e-6	1e-6	1e-6	1e-6
Epochs	1500	1500	1500	1500	1500	1500	1500	1500
Learning rate	5e-4	1e-4	5e-4	5e-4	5e-4	5e-4	5e-4	5e-4
Batch size	8	8	8	8	8	8	8	8
Ema decay	0.999	0.999	0.999	0.999	0.999	0.999	0.999	0.999
Energy coefficient λ_E	1	1	1	1	2	1	1	1
Force coefficient λ_F	80	80	80	100	20	80	80	20
Probability of optimizing AniDS p_{AniDS}	0.25	0.25	0.25	0.25	0.25	0.25	0.125	0.25
Denoise coefficient $\lambda_{Denoise}$	5	5	5	5	5	5	5	5
Corruption ratio r_{AniDS}	0.25	0.25	0.25	0.25	0.25	0.25	0.25	0.25

Table 9: Hyper-parameters for fine-tuning on rMD17 dataset.

Hyper-parameter	Aspirin	Benzene	Toluene	Uracil
Optimizer	AdamW	AdamW	AdamW	AdamW
Learning rate scheduling	Cosine	Cosine	Cosine	Cosine
Warm epochs	10	10	10	10
Weight decay	1e-6	1e-6	1e-6	1e-6
Epochs	2000	2000	2000	2000
Learning rate	2e-4	1e-4	2e-4	2e-4
Batch size	2	2	2	2
Energy coefficient λ_E	1	1	1	1
Force coefficient λ_F	80	80	80	20
Probability of optimizing AniDS p_{AniDS}	0.25	0.25	0.125	0.25
Denoise coefficient $\lambda_{Denoise}$	5	5	5	5
Corruption ratio r_{AniDS}	0.25	0.25	0.25	0.25

C.2.2 Supervised Learning with Partial Corruption and Auxiliary Denoising

OC22 For OC22, we employed the code and hyperparameters provided by DeNS [27], with a comprehensive list of training parameters presented in Table 10 and Table 11. It is important to note that, as we utilized a pre-trained model, we initially trained only the noise generator using KL loss to ensure training stability. This separate training phase continued until the generated KL loss

consistently fell below a threshold of 2.0, after which the entire model was trained. We performed this training on 4 NVIDIA A100 GPUs (80G). We also found that incorporating AniDS as an *auxiliary denoising objective* helps the VAE learn more informative noise generation from the provided force and energy supervision. In this configuration, we set $\lambda_\gamma = 0$ to simplify optimization, but a larger value may further enhance the anisotropic regularization effect and improve noise modeling performance. The pseudocode for this training process is similar to that provided in 2.

Table 10: Hyper-parameters for OC22 dataset.

Hyper-parameters	Value or description
Optimizer	AdamW
Learning rate scheduling	Cosine learning rate with linear warmup
Warmup epochs	0.002
Maximum learning rate	4×10^{-5}
Batch size (per gpu)	2
Number of epochs	1
Weight decay	1×10^{-3}
Dropout rate	0.1
Stochastic depth	0.1
Energy coefficient λ_E	4
Force coefficient λ_F	100
Gradient clipping norm threshold	50
Model EMA decay	0.999
Probability of optimizing AniDS p_{AniDS}	0.5
Denoise coefficient $\lambda_{Denoise}$	25
KL loss coefficient λ_{KL}	5
Prior distribution σ_p	0.15
Corruption ratio r_{AniDS}	0.5
Regularizer weight λ_γ	0.0

Table 11: Model hyper-parameters for OC22 dataset.

Model Hyper-parameters	Noise Generator	Denoising Autoencoder
Cutoff radius (\AA)	12	12
Maximum number of neighbors	20	20
Number of radial bases	32	600
Dimension of hidden scalar features in radial functions d_{edge}	(0, 64)	(0, 128)
Maximum degree L_{max}	2	6
Maximum order M_{max}	2	2
Number of Transformer blocks	4	18
Embedding dimension d_{embed}	(2, 64)	(6, 128)
$f_{ij}^{(L)}$ dimension d_{attn_hidden}	(2, 32)	(6, 64)
Number of attention heads h	4	8
$f_{ij}^{(0)}$ dimension d_{attn_alpha}	(0, 32)	(0, 64)
Value dimension d_{attn_value}	(2, 8)	(6, 16)
Hidden dimension in feed forward networks d_{ffn}	(2, 64)	(6, 128)
Resolution of point samples R	14	18

MPtrj On MPtrj, we employed two distinct models to validate the effectiveness of AniDS. First, GeoMFormer was trained from scratch on MPtrj, utilizing AniDS for auxiliary training; its parameters are detailed in Table 14 and Table 15. Second, similar to our approach for OC22, we performed continued training on the eqV2-S-DeNS model provided in Omat24 (which was exclusively trained on MPtrj). For this model, we adopted the same KL loss regularization strategy as for OC22 to ensure training stability, with its parameters specified in Table 12 and Table 13. Both models were trained on 8 NVIDIA A100 GPUs (40GB). The pseudocode for this training process is similar to that provided in 2.

C.3 Dynamic Simulation Tasks

We conducted a geometry optimization task using our model on the Aspirin subset of MD17. Specifically, we randomly selected 15 equilibrium structures and employed our force predictor

Table 12: Hyper-parameters for MPtrj dataset (EqV2).

Hyper-parameters	Value or description
Optimizer	AdamW
Learning rate scheduling	Cosine learning rate with linear warmup
Warmup epochs	0.1
Maximum learning rate	5×10^{-5}
Batch size (per gpu)	3
Number of epochs	7
Weight decay	1×10^{-3}
Energy coefficient λ_E	5
Force coefficient λ_F	20
stress isotropic coefficient λ_{S_iso}	5
stress anisotropic coefficient λ_{S_ani}	5
Probability of optimizing AniDS p_{AniDS}	0.5
Denoise coefficient $\lambda_{Denoise}$	10
KL loss coefficient λ_{KL}	10
Prior distribution σ_p	0.1
Corruption ratio r_{AniDS}	1.0
Regularizer weight λ_γ	0.0

Table 13: Model hyper-parameters for MPtrj dataset (EqV2).

Model Hyper-parameters	Noise Generator	Denoising Autoencoder
Cutoff radius (\AA)	12	12
Maximum number of neighbors	20	20
Dimension of hidden scalar features in radial functions d_{edge}	(0, 64)	(0, 128)
Maximum degree L_{max}	4	4
Maximum order M_{max}	2	2
Number of Transformer blocks	2	8
Embedding dimension d_{embed}	(4, 32)	(4, 128)
$f_{ij}^{(L)}$ dimension d_{attn_hidden}	(4, 32)	(4, 64)
Number of attention heads h	4	8
$f_{ij}^{(0)}$ dimension d_{attn_alpha}	(0, 32)	(0, 64)
Value dimension d_{attn_value}	(4, 8)	(4, 16)
Hidden dimension in feed forward networks d_{ffn}	(4, 64)	(4, 128)
Resolution of point samples R	18	18

Table 14: Hyper-parameters for MPtrj dataset (GeoMFormer).

Hyper-parameters	Value or description
Optimizer	Adam
Learning rate scheduling	linear
Warmup epochs	1
Maximum learning rate	2×10^{-4}
Batch size (per gpu)	40
Number of epochs	50
Energy coefficient λ_E	1
Force coefficient λ_F	1
Probability of optimizing AniDS p_{AniDS}	0.25
Denoise coefficient $\lambda_{Denoise}$	0.8
KL loss coefficient λ_{KL}	1e-3
Prior distribution σ_p	0.05
Corruption ratio r_{AniDS}	0.25
Regularizer weight λ_γ	0.0

(EquiformerV2 + AniDS) to optimize their geometries. The optimized configurations were then

Table 15: Model hyper-parameters for MPtrj dataset (GeoMFormer).

Model Hyper-parameters	Noise Generator	Denoising Autoencoder
Cutoff radius (Å)	5	5
Maximum number of expanded atoms	256	256
Number of radial bases	10	10
Number of Transformer layers	2	6
Embedding dimension d_{embed}	128	128
Number of attention heads h	8	8
Hidden dimension in feed forward networks d_{ffn}	128	128

compared against reference structures obtained via DFT geometry optimization, and we evaluated the RMSD between corresponding atomic positions.

Because the original MD17 dataset used the FHI-aims package with the PBE-vdW-TS functional under tight settings—which is subject to licensing restrictions—we performed our DFT-based geometry optimizations using PySCF at the PBE-D3BJ/def2-SVP level. This setup provides comparable accuracy in molecular geometries while remaining fully open-source.

All models were fine-tuned on the same training samples and evaluated on the same 15 randomly selected equilibrium structures from the Aspirin subset. Table 16 summarizes the RMSD improvements (i.e., reductions in atomic positional deviations before vs. after optimization) under three configurations.

As shown in the table, all three models achieve comparable RMSD improvements, with AniDS exhibiting the largest average reduction. While the absolute differences are modest, partly due to the limited optimization steps used in this evaluation.

Table 16: Comparison of RMSD improvement across different denoising strategies.

Structure Index	AniDS	DeNS	No Denoising
1	0.0829	0.0788	0.0653
2	0.0650	0.0655	0.0650
3	0.2911	0.2895	0.2869
4	0.1883	0.1879	0.1808
5	0.1830	0.1827	0.1827
6	0.0668	0.0664	0.0663
7	0.1083	0.1075	0.1083
8	0.0925	0.0926	0.0922
9	0.2478	0.2445	0.2589
10	0.0741	0.0821	0.0819
11	0.0887	0.0886	0.0893
12	0.0637	0.0637	0.0673
13	0.1197	0.1167	0.1185
14	0.1441	0.1438	0.1438
15	0.0876	0.0868	0.0862
Average	0.1269	0.1265	0.1262

C.4 Dataset License

The datasets used in our experiments are released under the following licenses:

- **PCQM4Mv2:** Creative Commons Attribution 4.0 International License (CC BY 4.0)
- **MD17:** MIT License
- **MPtrj:** MIT License
- **OC22:** Creative Commons Attribution 4.0 International License (CC BY 4.0)
- **ALEXANDRIA:** Creative Commons Attribution 4.0 International License (CC BY 4.0)

D Pseudo Code

Algorithm 1 Pretrain with AniDS

Require: λ_{AniDS} , λ_{KL} , λ_γ , κ , σ_p
Require: Noise Decoder GNN, Noise Generator GNG

```

1: while training do
2:    $L_{\text{total}} \leftarrow 0$ 
3:   Sample a batch of  $B$  structures  $\{S^{(j)}\}_{j=1}^B$ 
4:   for  $j$  to  $B$  do ▷ This for loop can be parallelized
5:      $S^{(j)} = \{(z_i, p_i)\}_{i=1}^{N_j}$ ,  $L_{\text{KL}} \leftarrow 0$ ,  $L_\gamma \leftarrow 0$ 
6:     for  $i$  = 1 to  $N_j$  do ▷ This for loop can be parallelized
7:        $(\Sigma_i, \Gamma_i) \leftarrow \text{GNG}(S^{(j)})$  ▷  $\Gamma_i = \sum_k \gamma_{ik}$  (anisotropic mass)
8:        $L_i \leftarrow \text{Cholesky}(\Sigma_i)$ 
9:       Sample  $\epsilon_i \sim \mathcal{N}(0, \mathbf{I}_3)$ ,  $\tilde{p}_i \leftarrow p_i + L_i \epsilon_i$ 
10:       $L_{\text{KL}} \leftarrow L_{\text{KL}} + \text{KL}(\sigma_p \mathbf{I}, \Sigma_i)$ 
11:       $L_\gamma \leftarrow L_\gamma + [\max(0, \kappa - \Gamma_i)]^2$ 
12:    end for
13:     $\tilde{S}^{(j)} \leftarrow \{(\tilde{z}_i, \tilde{p}_i)\}_{i=1}^{N_j}$ 
14:     $\hat{\epsilon} \leftarrow \text{GNN}(\tilde{S}^{(j)})$ 
15:     $L_{\text{AniDS}} \leftarrow \frac{1}{N_j} \sum_{i=1}^{N_j} \|L_i^{-T} \epsilon_i - \hat{\epsilon}_i\|_2^2$  ▷ Equivalent to Eq. 9
16:     $L_{\text{KL}} \leftarrow \frac{1}{N_j} L_{\text{KL}}$ ,  $L_\gamma \leftarrow \frac{1}{N_j} L_\gamma$ 
17:     $L_{\text{total}} \leftarrow L_{\text{total}} + \lambda_{\text{AniDS}} L_{\text{AniDS}} + \lambda_{\text{KL}} L_{\text{KL}} + \lambda_\gamma L_\gamma$ 
18:  end for
19:   $L_{\text{total}} \leftarrow \frac{L_{\text{total}}}{B}$ 
20:  Update GNN using  $L_{\text{total}}$ 
21: end while

```

E Computational Cost and Training Efficiency

To quantify the additional computational overhead introduced by AniDS, we compare training efficiency and model complexity across different noise-modeling choices on rMD17 (Aspirin, 50 training structures). Results are summarized in Table 17.

Table 17: Model size and per-epoch training time on rMD17 (Aspirin, 50 train) on single NVIDIA H100 GPU.

Method	#Parameters	Training Time per Epoch (s)
EqV2 (No Noise)	6.35M	6.2
EqV2 + DeNS	6.35M	6.9
EqV2 + DenoiseVAE	7.20M	7.3
EqV2 + AniDS (Ours)	7.36M	7.3

As shown, AniDS incurs a moderate increase in model size and training time, primarily due to its more expressive, structure-aware noise generator that outputs full covariance matrices. This overhead is justified by the significant performance gains reported in our main results (lowest MAE among all baselines).

Algorithm 2 Training with AniDS

Require: $p_{\text{AniDS}}, \lambda_{\text{AniDS}}, r_{\text{AniDS}}, \lambda_E, \lambda_F, \lambda_{\text{KL}}, \lambda_\gamma, \kappa, \sigma_p$
Require: Noise Decoder GNN, Noise Generator GNG

```

1: while training do
2:    $L_{\text{total}} \leftarrow 0$ 
3:   Sample a batch of  $B$  structures  $\{S_{\text{non-eq}}^{(j)}\}_{j=1}^B$ 
4:   for  $j = 1$  to  $B$  do ▷ This for loop can be parallelized
5:      $S_{\text{non-eq}}^{(j)} = \{(z_i, p_i, f_i)\}_{i=1}^{N_j}$ 
6:      $L_{\text{KL}} \leftarrow 0, L_\gamma \leftarrow 0$ 
7:     Sample  $u \sim \mathcal{U}(0, 1)$ 
8:     if  $u < p_{\text{AniDS}}$  then ▷ Decide whether to add noise to the structure
9:       for  $i = 1$  to  $N_j$  do ▷ Atom-wise partial corruption
10:       $(\Sigma_i, \Gamma_i) \leftarrow \text{GNG}(S_{\text{non-eq}}^{(j)})$ 
11:      Sample  $q_i \sim \mathcal{U}(0, 1); m_i \leftarrow \mathbb{1}[q_i < r_{\text{AniDS}}]$ 
12:      if  $m_i = 1$  then
13:         $L_i \leftarrow \text{Cholesky}(\Sigma_i); \text{ Sample } \epsilon_i \sim \mathcal{N}(0, \mathbf{I}_3)$ 
14:         $\tilde{p}_i \leftarrow p_i + L_i \epsilon_i$ 
15:      else
16:         $\tilde{p}_i \leftarrow p_i$ 
17:      end if
18:       $\tilde{f}_i \leftarrow f_i \cdot m_i$  ▷ Force encoding only for corrupted atoms
19:       $L_{\text{KL}} \leftarrow L_{\text{KL}} + \text{KL}(\sigma_p \mathbf{I}, \Sigma_i) \cdot m_i$ 
20:       $L_\gamma \leftarrow L_\gamma + [\max(0, \kappa - \Gamma_i)]^2 \cdot m_i$ 
21:    end for
22:     $M_j \leftarrow \max\left(1, \sum_{i=1}^{N_j} m_i\right)$ 
23:     $\tilde{S}_{\text{non-eq}}^{(j)} \leftarrow \{(z_i, \tilde{p}_i)\}_{i=1}^{N_j}, \tilde{F}^{(j)} \leftarrow \{\tilde{f}_i\}_{i=1}^{N_j}$ 
24:     $(\hat{E}, \hat{F}, \hat{\epsilon}) \leftarrow \text{GNN}(\tilde{S}_{\text{non-eq}}^{(j)}, \tilde{F}^{(j)})$ 
25:     $L_E \leftarrow |E(S_{\text{non-eq}}^{(j)}) - \hat{E}|$ 
26:     $L_{\text{AniDS}} \leftarrow \frac{1}{M_j} \sum_{i=1}^{N_j} m_i \|L_i^{-T} \epsilon_i - \hat{\epsilon}_i\|_2^2$  ▷ Eq. 9 form
27:     $L_F \leftarrow \frac{1}{N_j} \sum_{i=1}^{N_j} (1 - m_i) \|f_i - \hat{f}_i\|_2^2$ 
28:     $L_{\text{KL}} \leftarrow \frac{1}{M_j} L_{\text{KL}}, L_\gamma \leftarrow \frac{1}{M_j} L_\gamma$ 
29:     $L_{\text{total}} \leftarrow L_{\text{total}} + \lambda_E L_E + \lambda_{\text{AniDS}} L_{\text{AniDS}} + \lambda_F L_F + \lambda_{\text{KL}} L_{\text{KL}} + \lambda_\gamma L_\gamma$ 
30:  else
31:     $(\hat{E}, \hat{F}) \leftarrow \text{GNN}(S_{\text{non-eq}}^{(j)})$ 
32:     $L_E \leftarrow |E(S_{\text{non-eq}}^{(j)}) - \hat{E}|$ 
33:     $L_F \leftarrow \frac{1}{N_j} \sum_{i=1}^{N_j} \|f_i - \hat{f}_i\|_2^2$ 
34:     $L_{\text{total}} \leftarrow L_{\text{total}} + \lambda_E L_E + \lambda_F L_F$ 
35:  end if
36: end for
37:  $L_{\text{total}} \leftarrow \frac{L_{\text{total}}}{B}$ 
38: Update GNN using  $L_{\text{total}}$ 
39: end while
  
```
